

Quantifying the Mesoscale Rectification of Latent Heat Flux

A THESIS SUBMITTED TO THE GRADUATE DIVISION OF THE UNIVERSITY OF
HAWAII AT MĀNOA IN PARTIAL FULFILLMENT OF THE REQUIREMENTS FOR
THE DEGREE OF

MASTER OF SCIENCE

IN

OCEANOGRAPHY

May 11, 2022

By
Bailey Donaldson

Thesis Committee:

Niklas Schneider, Chairperson
Bo Qiu,
Malte Stuecker,

Keywords: latent heat flux, rectify, mesoscale

Abstract

Ocean mesoscale fronts and eddies can impact large scale features due to nonlinear rectification. This project quantifies the rectification of ocean mesoscale sea surface temperature, wind speed, and specific humidity to the large-scale latent heat flux. We quantified nonlinearities caused by (1) the Clausius Clapeyron relation, (2) the positive correlation of sea surface temperatures and wind speed at the mesoscale, and (3) the covariability of wind speed and specific humidity. A Taylor Expansion to the second order of the latent heat flux around the large-scale wind speed, sea surface temperature, and specific humidity is used to estimate the nonlinear rectification of the three nonlinearities for the Gulf Stream, Kuroshio Extension, and Agulhas Return Current. We conducted two trials. Trial 1 utilized satellite observations of wind speed, sea surface temperature, and an estimated specific humidity to calculate nonlinearity (1) and (2). Trial 2 utilized ERA5 reanalysis of wind speed, sea surface temperature, and specific humidity to calculate all three nonlinearities. The average of the rectification terms are small for each trial, and generally range from -0.5 to $1.8 W/m^2$ with some regional exceptions. Results indicate that in Trial 1, the rectification from Clausius Clapeyron ranges from 0.09 to $3.85 W/m^2$ and the rectification from the sea surface temperature-wind covariability ranges from -4.06 to $4.39 W/m^2$ depending on the

region. In Trial 2, the rectification from Clausius Clapeyron ranges from 0.05 to 3.74 W/m^2 , the sea surface temperature-wind covariability ranges from -14.92 to 14.19 W/m^2 , and the wind-specific humidity covariability ranges from -9.30 to 7.91 W/m^2 . Results find that the Clausius Clapeyron term exhibits a dependence on background wind speed and both covariability terms exhibit a dependence on wind direction. All rectification terms exhibit a strong dependence on filter size and humidity. The Taylor Expansion in Trial 1 had a low error, however, the results from Trial 2 were highly variable and exhibited a large error that is directly related to the Clausius Clapeyron term. On large spatial and temporal averages, the rectification is modest but can be important at times over strong mesoscale sea surface temperature variance and under particular background wind conditions.

Contents

1	List of Tables	1
2	List of Figures	2
3	Introduction	3
3.1	Types of Nonlinearities	4
4	Methods	4
4.1	Regions of Study	4
4.2	Data	5
4.3	Heat Flux Calculation	5
4.3.1	Humidity	6
4.4	Large Scale and Mesoscale Separation	7
4.5	Taylor Expansion	8
5	Results	9
5.1	Trial 1: Satellite Data	9
5.1.1	Seasonal Cycle	14
5.1.2	Rectification Dependence on Wind and SST	18
5.1.3	Filter Size Dependence	20
5.1.4	ε	21
5.2	Trial 2: Reanalysis Data	22
5.2.1	Trial 1 and Trial 2 Comparison	27
5.2.2	Seasonal Cycle	28
5.2.3	Rectification Dependence on Wind, SST, and Humidity	29
5.2.4	ε	31
5.2.5	Linearize around Relative Humidity vs. Specific Humidity	33
5.2.6	Drag and Stability Coefficients	35
6	Conclusion	36
7	Discussion	38

1 List of Tables

Table 1: Trial 1 Rectification Mean, Maximum, and Minimum	12
Table 2: Trial 1 Filter Size Comparison	21
Table 3: Trial 1 ε Mean, Maximum, and Minimum	22
Table 4: Trial 2 Rectification Mean, Maximum, and Minimum	23
Table 5: Trial 2 ε Mean, Maximum, and Minimum	32

2 List of Figures

Figure 1: Comparison of Specific Humidity	6
Figure 2: Trial 1 Daily Wind Speed, SST, and Large Scale LHF	10
Figure 3: Trial 1 Daily Rectification and Rectification Percent	11
Figure 4: Trial 1 Monthly Rectification	12
Figure 5: Trial 1 Maps of Rectification	13
Figure 6: Trial 1 Daily Rectification and Variables in Gulf Stream 2004	15
Figure 7: Trial 1 Rectification Dependence on SST and Wind Speed	16
Figure 8: Trial 1 Rectification Dependence on SST and Wind Direction	17
Figure 9: Trial 1 Second Derivative Dependence on SST and Wind Speed	18
Figure 10: Trial 1 U'T' Covariance and SST Standard Deviation Dependence	19
Figure 11: Trial 1 Filter Size Comparison	20
Figure 12: Trial 1 Daily ε	22
Figure 13: Trial 2 Daily Rectification and Variables in Gulf Stream	24
Figure 14: Trial 2 Daily Rectification and Variables in Kuroshio Extension	24
Figure 15: Trial 2 Daily Rectification and Variables in Agulhas Return Current	25
Figure 16: Trial 2 Monthly Rectification	25
Figure 17: Trial 2 Maps of Rectification	26
Figure 18: Trial 1 and Trial 2 Comparison of Variables	27
Figure 19: Trial 2 Daily Large Scale LHF	28
Figure 20: Trial 2 Rectification Dependence on SST and Wind Speed	29
Figure 21: Trial 2 Q_{CC} Dependence on SST and Wind Speed	30
Figure 22: Trial 2 Q_{UT} Dependence on Specific Humidity and Wind Direction	31
Figure 23: Trial 2 Q_{UH} Dependence on Specific Humidity and Wind Direction	32
Figure 24: Trial 2 Rectification Percentage	33
Figure 25: Trial 2 Daily ε	34
Figure 26: Trial 2 ε Dependence on Rectification	35
Figure 27: Trial 2 Large Scale LHF Comparison with ERA5	37

3 Introduction

The atmosphere and ocean are closely related. They force one another in a complex relationship that changes with temporal and spatial scale. The advent of satellite observations at small spatial resolutions opened up the ability to study ocean-atmosphere interaction at the oceanic mesoscale (100 to 1000 km) (Chelton and Xie, 2010). One interesting course of study is the impact of mesoscale ocean features on the atmosphere. At the large-scale, the atmosphere modifies the ocean through wind stress and turbulent heat fluxes; however, at the mesoscale, the ocean drives the atmosphere (e.g., Chelton and Xie, 2010; Small et al., 2008).

The impact the mesoscale features have on the large-scale circulation of the atmosphere is in its early stages of study. Recent studies found that ocean mesoscale eddies rectify to impact the large-scale atmosphere. If a model is run twice, once with mesoscale features present and the other with the features removed, there is an impact on the large-scale atmosphere. For example, Foussard et al. (2019) ran an experiment of a sea surface temperature (SST) field in an idealized rectangular channel with and without mesoscale eddies. They found a poleward shift of both the storm track and the eddy-driven jet in the experiment with eddies present. A similar study was conducted by Piazza et al. (2016) in the Gulf Stream in which they found an impact from ocean mesoscale features on the subtropical jet stream, the Atlantic storm track, and Rossby wave breaking frequency. Similar studies have been conducted around this topic focused on the Kuroshio Extension (e.g., Putrasahan et al., 2013; Ma et al., 2015).

The turbulent heat fluxes are one source of the rectification that links the ocean mesoscale to the atmospheric large scale. Sensible heat flux (SHF) and latent heat flux (LHF) are a major link between the ocean and atmosphere. They drive the global heat budget and are the main process by which the ocean releases heat into the atmosphere (Cayan, 1992). SHF and LHF depend on wind speed, SST, humidity, and air temperature. Mesoscale oceanic features modify the atmosphere by changing wind, clouds, and rainfall, and thus, they also modify SHF and LHF (Frenger et al., 2013).

Heat fluxes produce a rectified effect in that they modify cold core eddies differently from warm core eddies (e.g., Liu et al., 2018; Leyba et al., 2017; Villas Bôas et al., 2015). Anticyclonic and cyclonic eddies generate downwelling and upwelling that create positive and negative SST anomalies, respectively (e.g., Frenger et al., 2013). Cold core eddies generate negative heat flux anomalies such that the ocean gains heat from the atmosphere. Warm core eddies do the opposite such that there are positive heat flux anomalies indicating heat gain to the atmosphere. However, more heat is lost over warm core eddies than is gained over a cold eddy with the same magnitude SST perturbation resulting in a net surface heating of the atmosphere (e.g., Foussard et al., 2019; Villas Bôas et al., 2015; Leyba et al., 2017; Liu et al., 2018, 2020). This occurs due to nonlinearities in the heat fluxes. We will quantify the nonlinearities that rectify mesoscale SST, wind speed, and specific humidity to large scale latent heat flux in this thesis.

3.1 Types of Nonlinearities

There are three nonlinearities that we will be quantifying in our analysis, two of which are well studied. The first is the nonlinearity caused by the Clausius Clapeyron relation. Clausius Clapeyron is a nonlinear relationship between temperature and saturation vapor pressure, which the heat fluxes depend on. Saturation vapor pressure increases exponentially with increase in temperature (Wallace and Hobbs, 2006). It is the nonlinearity most commonly thought to cause the rectification (Ma et al., 2017).

The second nonlinearity is due to the covariability of wind speed and SST. The covariability is scale dependent. At the large-scale, greater wind speed drives an increase in evaporative cooling resulting in a negative correlation between wind speed and SST (e.g., Chelton et al., 2004; Chelton and Xie, 2010; Small et al., 2008). At the mesoscale, the vertical mixing mechanism and the pressure adjustment mechanism result in a positive wind speed and SST correlation (e.g., Liu et al., 2018; Putrasahan et al., 2013; O’Neill et al., 2010). Numerous studies show that there is a strong correlation between mesoscale ocean features and wind speed (e.g., Chelton and Xie, 2010; Frenger et al., 2013; Chelton et al., 2004; O’Neill et al., 2010). The multiplication of wind speed and SST in the LHF equation results in a rectification.

The third nonlinearity is due to the covariability of specific humidity and wind speed. Due to the lack of satellite observations of specific humidity, this relationship is not well documented. However, we will consider it because this nonlinearity is mathematically significant in this study.

The rectification of mesoscale features to large scale surface heat flux has been quantified in Sroka et al. (2022). This research project similarly quantified the rectification of ocean mesoscale SST, wind speed, and specific humidity to the large-scale LHF. They found that the rectification was modest, but could reach $5 W/m^2$ north of the Kuroshio Extension. We also quantified the three nonlinearities listed above. However, unlike Sroka et al. (2022), we utilized a Taylor Expansion to the second order of the latent heat flux around a background state of wind speed, SST, and specific humidity. This allows us to separate the nonlinearities unlike in Sroka et al. (2022) where they are considered as a whole. We explored which nonlinearity, if any, is the most predominant. We also explored which weather conditions are favorable for larger rectification and if the rectification has a locational dependence.

4 Methods

4.1 Regions of Study

We hypothesized that rectification will be greater in regions with abundant mesoscale features. Thus, we studied the Kuroshio Extension region (140.875°E to 179.875°E and 35.875°N to 43.635°N), the Agulhas Return Current region (44.625°S to 38.875°S and 11.375°E to 58.125°E), and the Gulf Stream (36°N to 47.75°N and 289°W to 323.75°W (or 71°W to 36.25°W)). These regions have a strong tropospheric response to mesoscale SST features (Chelton and Xie, 2010; O’Neill et al., 2005). In the Kuroshio Extension and Gulf

Stream, the effect of the strong oceanic currents can impact wind stress in excess of 20% (Chelton et al., 2004). This indicates that these regions are characterized by a strong positive correlation between wind speed and SST (Chelton and Xie, 2010; O’Neill et al., 2005). The Kuroshio Extension, in particular, is useful to study because it was used in numerous recent studies which found the impact of mesoscale eddy activity on the large scale (e.g., Ma et al., 2015; Putrasahan et al., 2013; Sroka et al., 2022).

4.2 Data

To calculate the air-sea latent heat flux, the following data is necessary: SST, wind speed, and specific humidity. Our study utilized satellite data in Trial 1 and ERA5 Reanalysis data in Trial 2. Both trials studied the data over the period from January 1st, 2003 to December 31st, 2008 projected onto a $0.25^\circ \times 0.25^\circ$ grid.

In our first trial, only satellite product was used. The limitations of using satellite data were that specific humidity is unknown. The details of how this limitation was remediated is discussed in the Humidity section on page 6. Wind speed (U_{10} or U) at the reference height of 10 m was obtained from the Quick Scatterometer (Quikscat) (Ricciardulli et al., 2011). SST was obtained from version 7 running 3-day averages of the Advanced Microwave Scanning Radiometer for EOS (ASMR-E) (Wentz et al., 2014). Quikscat and ASMR-E are produced by Remote Sensing Systems and were sponsored by the NASA AMSR-E Science Team and the NASA Earth Science MEaSUREs Program. Data is available at www.remss.com. Quikscat wind speed data was recorded twice a day during ascending and descending tracks. Our calculations use the average of both tracks. These two datasets are useful to us because they have been used frequently in important studies regarding the covariability of wind speed and SST (e.g., Chelton et al., 2004; Chelton and Xie, 2010; Small et al., 2008).

In our second trial, we used the ERA5 reanalysis data downloaded from the Copernicus Climate Change Service (C3S) Climate Data Store (Hersbach et al., 2019b,a). The data downloaded includes sea surface temperature (T_s), the surface wind vector ($[u, v]$) at 10 m, and specific humidity (q_a). Use of the reanalysis data served to confirm our results with the satellite data. The specific humidity data, which we lack in the first trial, also served to reveal if information was lost due to the assumptions made.

4.3 Heat Flux Calculation

We used the parameterization of the latent heat flux (LHF) equation by Fairall et al. (2003).

$$Q_{LHF} = L_v \rho_a C_E |U_{10}| (q_s - q_a). \quad (1)$$

The constants that follow were obtained from Wallace and Hobbs (2006). Latent heat of evaporation L_v is set to $2.5 \times 10^6 \text{ J kg}^{-1}$. The density of air at sea level ρ_a is assumed to be 1.178 kg m^{-3} . The stability coefficient is $C_E = 1.3 \times 10^{-3}$. Although LHF is stability dependent, the stability coefficient is difficult to quantify, thus, we set it as this constant value used in Wallace and Hobbs (2006). The stability coefficient, and the drag coefficient,

are nonlinear with respect to wind speed, thus they may also be a source of rectification (Smith, 1988; Ma et al., 2017). We will not quantify these nonlinearities in this paper, however, we will address their potential impacts in the Section 5.2.6. Again, the wind speed (U_{10}) and sea surface temperature (SST) are provided from the Quikscat scatterometer and ASMR-E data in the first trial and ERA5 reanalysis data in the second trial.

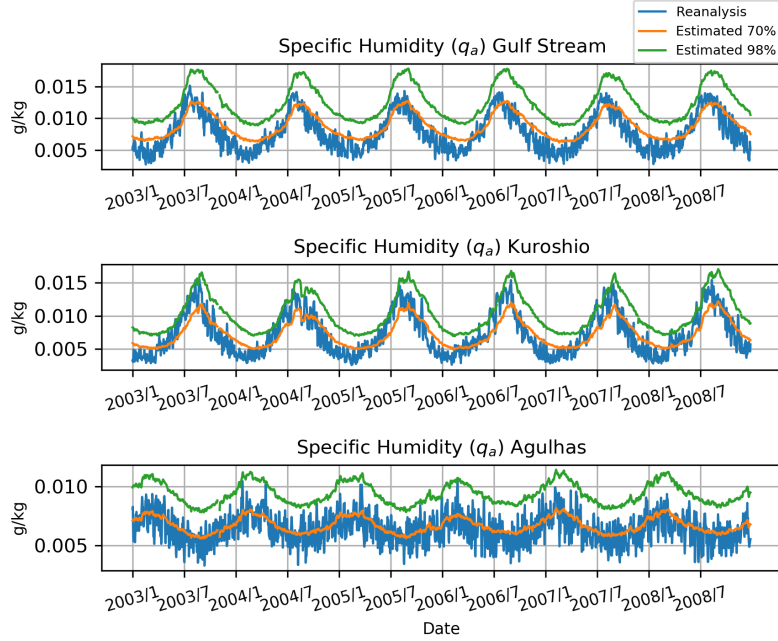


Figure 1: Comparison of specific humidity data. Daily and spatial average in the Gulf Stream, Agulhas Return Current, and Kuroshio Extension. The blue line indicates specific humidity provided by ERA5 reanalysis. The orange and green line indicate specific humidity, which is calculated by taking 70% or 98% of saturation humidity that was calculated with ASMR-E SST.

4.3.1 Humidity

To obtain saturation humidity (q_s), we calculate it using SST and equations for humidity and water vapor pressure (e) from Wallace and Hobbs (2006). The original equations from Wallace and Hobbs (2006) have been rearranged for simplification:

$$q_s = \left(\frac{M_w e}{p}\right) / \left(M_d - \frac{M_d e}{p} + \frac{M_w e}{p}\right), \quad (2)$$

$$e = 6.1094 \times e^{\frac{17.625T}{T+243.04}}. \quad (3)$$

Our constants are the total pressure of moist air ($p = 1026.8 \text{ hPa}$), the molecular weight of dry air ($M_d = 28.97 \text{ g}$), and the molecular weight of water ($M_w = 18.016 \text{ g}$) (Wallace and Hobbs, 2006).

Lastly, we require specific humidity. For our second trial, we can use specific humidity data from the ERA5 reanalysis. However, we are unable to obtain or calculate specific humidity from satellite data for our first trial. Instead, we assume that specific humidity is some percentage of the saturation humidity that we calculate with the ASMR-E SST. We compared our assumed specific humidity with the reanalysis specific humidity in Figure 1. Some literature has used 98% for their assumptions (e.g., Santorelli et al., 2011); however, we decided to use 70% because 98% overestimates the humidity when compared to the ERA5 humidity (see Figure 1). Due to this assumption of specific humidity, deviations from 70% that could be from mesoscale features, are lost. We will discuss the impacts of this assumption in the Results section.

4.4 Large Scale and Mesoscale Separation

In order to quantify the impact the mesoscale has on the large scale, we need to separate them from one another. We used a top hat filter to achieve this. We used a Reynolds decomposition to express our variables as the sum of the low pass filtered variable (e.g. $\bar{\star}$) and the high pass filtered variable (e.g. \star'), i.e. $\star = \bar{\star} + \star'$. The low pass filtered variable represents the background state and the high pass filtered variable encompasses all of the mesoscale anomalies.

We find the low pass filtered component of a data point by taking the mean of all the data in a dx by dy square (with area A) surrounding the original data point, then assign the mean to the center of the square (see Equation 4). The high pass filtered component is simply the difference between the low pass filtered component and the original data. Any operations performed between two high pass averaged values, are performed within the integral (see Equation 5):

$$\bar{\star} = \frac{1}{A} \int \int \star dydx, \quad (4)$$

$$\overline{\star'\diamond'} = \frac{1}{A} \int \int (\star - \bar{\star})(\diamond - \bar{\diamond}) dydx. \quad (5)$$

Note that under this mathematical convention, the following is true: $\overline{\star'} = 0$.

Much consideration was taken in the decision of the filter size. We wanted our filter to encompass as much mesoscale features as possible while removing all large scale features. Thus, we turned to literature to decide our filter size. A study was done by Laurindo et al. (2019) specifically to address the issue of deciding the cut off scale between the large scale and the ocean mesoscale. They used cross-spectral statistics between SST and wind speed observations globally to characterize the spectral linear relationship between the two variables. At the latitudes and basins of my three regions of study, the shift between the oceanic mesoscale and large scale is at about 1000 km. The 1000 km filter size suggested by Laurindo et al. (2019) is much larger compared to the filter sizes used in studies that separate the ocean mesoscale from the large scale. For example, in a study by Sroka et al. (2022), they isolated the impact of ocean mesoscale eddies on the turbulent heat fluxes in the Kuroshio Extension with a filter of 500 km. Studies by Ma et al. (2015) and Piazza et al.

(2016) analyzed the impact of mesoscale eddies on the large scale in the Kuroshio Extension and Gulf Stream. They used a filter size of about 800 km and 300 km, respectively. We have chosen a filter size of 805 km which is a balance between the classically chosen filter sizes and the filter size recommended by Laurindo et al. (2019).

Another method to determine the filter size is to use the covariability of wind speed anomalies and SST anomalies similarly to (Laurindo et al., 2019). Large scale SST and wind speed are negatively correlated at the large scale yet positively correlated at the mesoscale; thus, the magnitude and sign of the covariability term should inform us of the appropriate filter size. We found the filter size that results in the largest positive covariability of wind speed anomalies and SST anomalies. However, the result of this method was a filter size of 140 km x 140 km for the Kuroshio Extension and Agulhas Return Current. Literature claims that oceanic mesoscale features are generally range from 20km - 1000 km, thus, this filter is likely too small (Chelton et al., 2011). For our calculations, we decided to use the 805 km filter size. Further discussion about the impacts of filter size on our results will be explored in the Section 5.1.3.

4.5 Taylor Expansion

To quantify the magnitude of the rectification, we performed a Taylor Expansion of Q_{LHF} (see Equation 1) around a background-state of wind speed, SST, and specific humidity to the second order. The nonlinear terms contain the rectification. We take the low pass (denoted by the overbar) of the Taylor Expansion because we seek to understand how heat fluxes rectify to the large scale:

$$\begin{aligned}
\overline{Q(\bar{T} + T', \bar{U} + U', \bar{q}_a + q'_a)} &= Q(\bar{T}, \bar{U}, \bar{q}_a) + \frac{\partial Q}{\partial T} \Big|_{\bar{T}, \bar{U}, \bar{q}_a} \overline{T'} + \frac{\partial Q}{\partial U} \Big|_{\bar{T}, \bar{U}, \bar{q}_a} \overline{U'} \\
&+ \frac{\partial Q}{\partial q_a} \Big|_{\bar{T}, \bar{U}, \bar{q}_a} \overline{q'_a} + \frac{1}{2} \frac{\partial^2 Q}{\partial T^2} \Big|_{\bar{T}, \bar{U}, \bar{q}_a} \overline{T'^2} + \frac{\partial^2 Q}{\partial T \partial U} \Big|_{\bar{T}, \bar{U}, \bar{q}_a} \overline{T'U'} + \frac{\partial^2 Q}{\partial q_a \partial U} \Big|_{\bar{T}, \bar{U}, \bar{q}_a} \overline{q'_a U'} \\
&+ \frac{\partial^2 Q}{\partial q_a \partial T} \Big|_{\bar{T}, \bar{U}, \bar{q}_a} \overline{q'_a T'} + \frac{1}{2} \frac{\partial^2 Q}{\partial U^2} \Big|_{\bar{T}, \bar{U}, \bar{q}_a} \overline{U'^2} + \frac{1}{2} \frac{\partial^2 Q}{\partial q_a^2} \Big|_{\bar{T}, \bar{U}, \bar{q}_a} \overline{q'^2_a} + \varepsilon,
\end{aligned} \tag{6}$$

$$\begin{aligned}
\underbrace{\overline{Q(\bar{T} + T', \bar{U} + U', \bar{q}_a + q'_a)}}_{Q_0 \text{ (Large-Scale)}} &= \underbrace{Q(\bar{T}, \bar{U}, \bar{q}_a)}_{Q_1 \text{ (Background State)}} + \underbrace{\frac{1}{2} \frac{\partial^2 Q}{\partial T^2} \Big|_{\bar{T}, \bar{U}, \bar{q}_a} \overline{T'^2}}_{Q_{CC} \text{ (Clausius Clapeyron)}} + \\
&\underbrace{\frac{\partial^2 Q}{\partial T \partial U} \Big|_{\bar{T}, \bar{U}, \bar{q}_a} \overline{T'U'}}_{Q_{UT} \text{ (Covariability)}} + \underbrace{\frac{\partial^2 Q}{\partial q_a \partial U} \Big|_{\bar{T}, \bar{U}, \bar{q}_a} \overline{q'_a U'}}_{Q_{UH} \text{ (Covariability)}} + \varepsilon.
\end{aligned} \tag{7}$$

Equation 6 is the entire Taylor Expansion; however, many terms cancel out. Because $\bar{\kappa} = 0$, all of the linear terms are zero. It is also true that $\frac{\partial^2 Q}{\partial U^2} \Big|_{\bar{T}, \bar{U}, \bar{q}_a} = 0$ and $\frac{\partial^2 Q}{\partial q_a^2} \Big|_{\bar{T}, \bar{U}, \bar{q}_a} = 0$. Once removing the terms that are zero, we find Equation 7. Equation 7 will be used in our second trial when we use reanalysis data. In our first trial, we use satellite data and a constant specific humidity. Therefore, our Taylor Expansion is only around SST and wind speed and it can be simplified to Equation 8.

$$\underbrace{Q(\bar{T} + T', \bar{U} + U', \bar{q}_a)}_{Q_0 \text{ (Large-Scale)}} = \underbrace{Q(\bar{T}, \bar{U}, \bar{q}_a)}_{Q_1 \text{ (Background State)}} + \underbrace{\frac{1}{2} \frac{\partial^2 Q}{\partial T^2} \Big|_{\bar{T}, \bar{U}, \bar{q}_a} \bar{T}^2}_{Q_{CC} \text{ (Clausius Clapeyron)}} + \underbrace{\frac{\partial^2 Q}{\partial T \partial U} \Big|_{\bar{T}, \bar{U}, \bar{q}_a} \bar{T}' \bar{U}'}_{Q_{UT} \text{ (Covariability)}} + \varepsilon. \tag{8}$$

The terms on the left hand sides of Equations 6 - 8 have been denoted Q_0 and represent the large scale latent heat flux. The first term on the right hand side of Equations 6 - 8 have been denoted Q_1 and it represents the background state of latent heat flux. The distinction between Q_0 and Q_1 is small but important. The difference is the effect of the nonlinearities and the rectification. Note how Q_0 was calculated with dependence on the mesoscale features (T' , U' , (and q'_a)), while Q_1 has no dependence on the mesoscale features. Q_0 has been impacted by mesoscale rectification and Q_1 has not. Our nonlinearities are as follows: the nonlinearity from Clausius Clapeyron (Q_{CC}), the nonlinearity from the covariability of wind speed and SST (Q_{UT}), and the nonlinearity from the covariability of wind speed and specific humidity (Q_{UH}). These nonlinearities were described in more detail in Section 3.1. ε encompasses higher order terms and other residuals. It will be important to solve for this term to reveal if any nonlinearities, including the nonlinearity from the drag and stability coefficient, have been missed by our current analysis.

5 Results

5.1 Trial 1: Satellite Data

First, we plotted the daily and spatially averaged SST from ASMR-E, Quikscat wind speed, and large scale LHF (Q_0) to gain a better understanding of the climatology in Figure 2. Large scale LHF ranges from about 30 to 150 W/m^2 which is consistent with the average LHF from Fairall et al. (2003) which ranges from 40 to 250 W/m^2 . Positive values of LHF and rectification indicate heat loss from the ocean and heat gain to the atmosphere. As expected, both wind speed and SST exhibit a seasonal cycle such that SST peaks in the summer months and wind speed peaks in the winter months. The seasonal variability in the Agulhas Return Current ranges only about 5K and 5 m/s, which is less than the Gulf

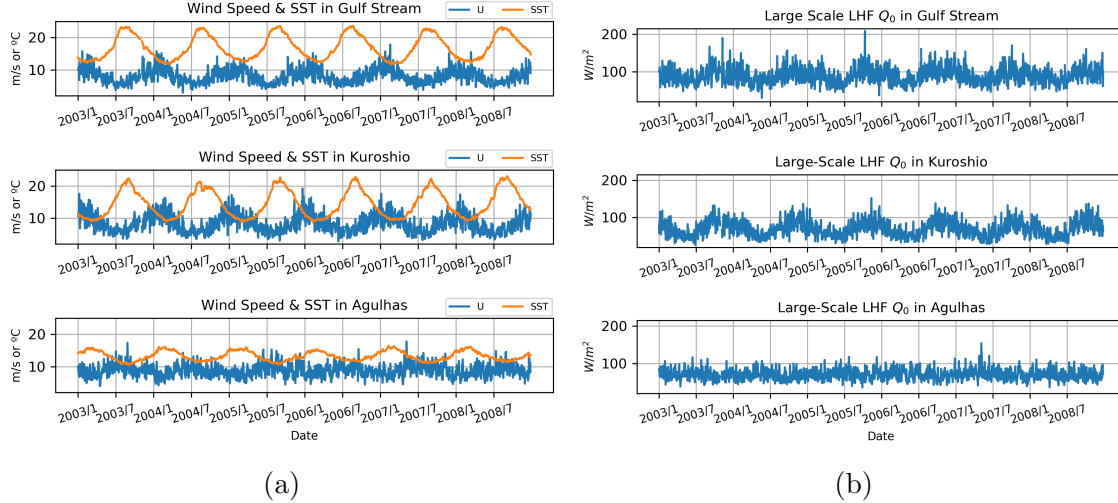


Figure 2: Trial 1. Daily and spatial average in the Gulf Stream, Agulhas Return Current, and Kuroshio Extension. (a) is of Quikscat wind speed (U) in blue and ASMR-E SST in orange. (b) is of large-scale LHF (Q_0).

Stream and Kuroshio Extension which vary by about 10K and 8 m/s. This is likely due to the larger amount of ocean cover in the Southern Hemisphere or the increased distance from land in the Agulhas Return Current, which both limit seasonal variability. The seasonal cycle is present in the large scale LHF due to its dependence on SST and wind speed.

The daily variability of SST for all regions is small as expected, however, the wind speed daily variability is large. When averaged spatially, the wind speed can vary by as much as 5 to 10 m/s over the course of a few days.

In our analysis we found that when specific humidity is estimated to be a percent of the saturation humidity, the specific humidity acts as a scaling term for all terms in the Taylor Expansion. In Section 4.3.1 we chose to use 70% of saturation humidity as our estimation for the specific humidity. If we increased relative humidity from 70% of saturation humidity to 98%, it decreased the large scale LHF and the rectification by a factor of 15. However, the percent the rectification makes up of the large scale LHF will remain the same. With a 98% assumption, the large scale LHF is decreased to a range of 2 to 10 W/m^2 in each region. Our 70% assumption is much closer to what is typically observed, 40 to 250 W/m^2 , thus we decided to use the 70% assumption. As mentioned in Section 4.3.1, some mesoscale variability will be lost due to our assumption. Due to the strong dependence on humidity, the humidity variability needs to be considered. We will do so in Trial 2 in Section 5.2.

Now that we have a grasp of the general climatology of each region and the large scale LHF, we can look at the rectification as calculated with Equation 8. We look to Figure 3, Figure 4, and Table 1 to quantify the rectification terms. On average, Clausius Clapeyron is about 1 to 2 W/m^2 and the covariability ranges from -0.4 to 0.49 W/m^2 depending on the region. Though the mean of the Clausius Clapeyron term is greater than the covariability term, the range of the covariability term exceeds the Clausius Clapeyron term. At the 5th

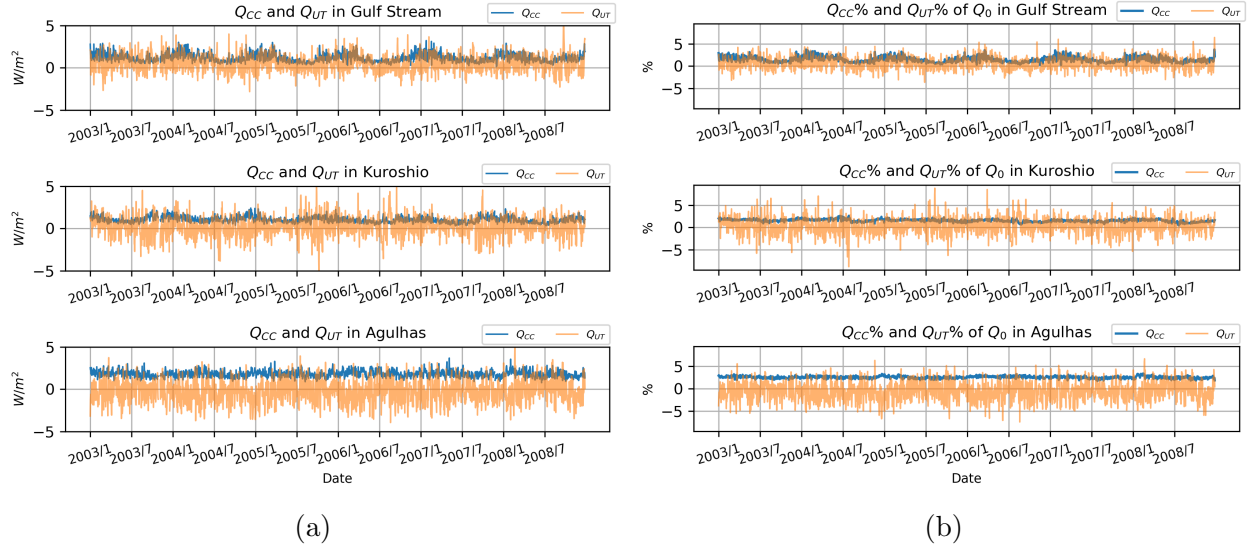


Figure 3: Trial 1. Daily and spatial average of the rectification in the Gulf Stream, Agulhas Return Current, and Kuroshio Extension. (a) is of the daily average of the Clausius Clapeyron term (Q_{CC}) and the covariability term (Q_{UT}). (b) is the percent Q_{CC} and Q_{UT} make up of the large scale LHF averaged daily. The blue lines represent the rectification from Q_{CC} and the orange lines represent the rectification from Q_{UT} .

and 95th percentile, the Clausius Clapeyron term ranges from 0.09 to 3.85 W/m^2 and the covariability term ranges from -4.06 to 4.39 W/m^2 . We must take note that in all the plots and tables where the mean is taken, the covariability term may appear small because it contains both positive and negative values.

	Gulf Stream (W/m^2)	Kuroshio (W/m^2)	Agulhas (W/m^2)
Q_0 mean	87.69	69.01	70.10
Q_0 max (95th%)	338.86 (146.87)	286.11 (124.65)	264.08 (111.03)
Q_0 min (5th%)	9.04 (41.47)	6.60 (29.34)	11.17 (37.05)
Q_{CC} mean	1.15	1.04	1.79
Q_{CC} max (95th%)	12.38 (3.85)	6.80 (2.15)	8.03 (3.26)
Q_{CC} min (5th%)	0.01 (0.09)	0.02 (0.35)	0.05 (0.70)
Q_{UT} mean	0.46	0.19	-0.40
Q_{UT} max (95th%)	20.47 (4.39)	14.51 (3.64)	16.44 (3.58)
Q_{UT} min (5th%)	-10.31 (-2.30)	-9.86 (-2.99)	-10.50 (-4.06)

Table 1: Trial 1. Mean, maximum and 95th percentile, minimum and 5th percentile of the large scale LHF (Q_0), the Clausius Clapeyron term (Q_{CC}), and the covariability of wind speed and SST (Q_{UT}) across the entire data set. Values are provided for the Gulf Stream, Kuroshio Extension, and Agulhas Return Current.

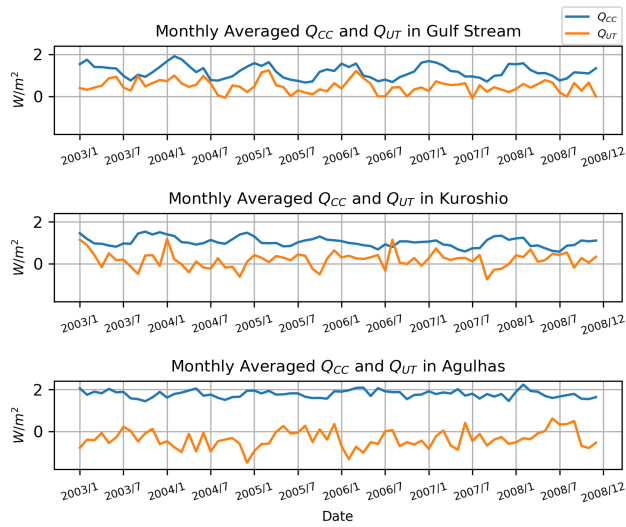


Figure 4: Trial 1. Spatial and monthly average of the rectification in the Gulf Stream, Agulhas Return Current, and Kuroshio Extension. The blue lines represent the rectification from the Clausius Clapeyron term (Q_{CC}) and the orange lines represent the rectification from the covariability of wind speed and SST (Q_{UT}).

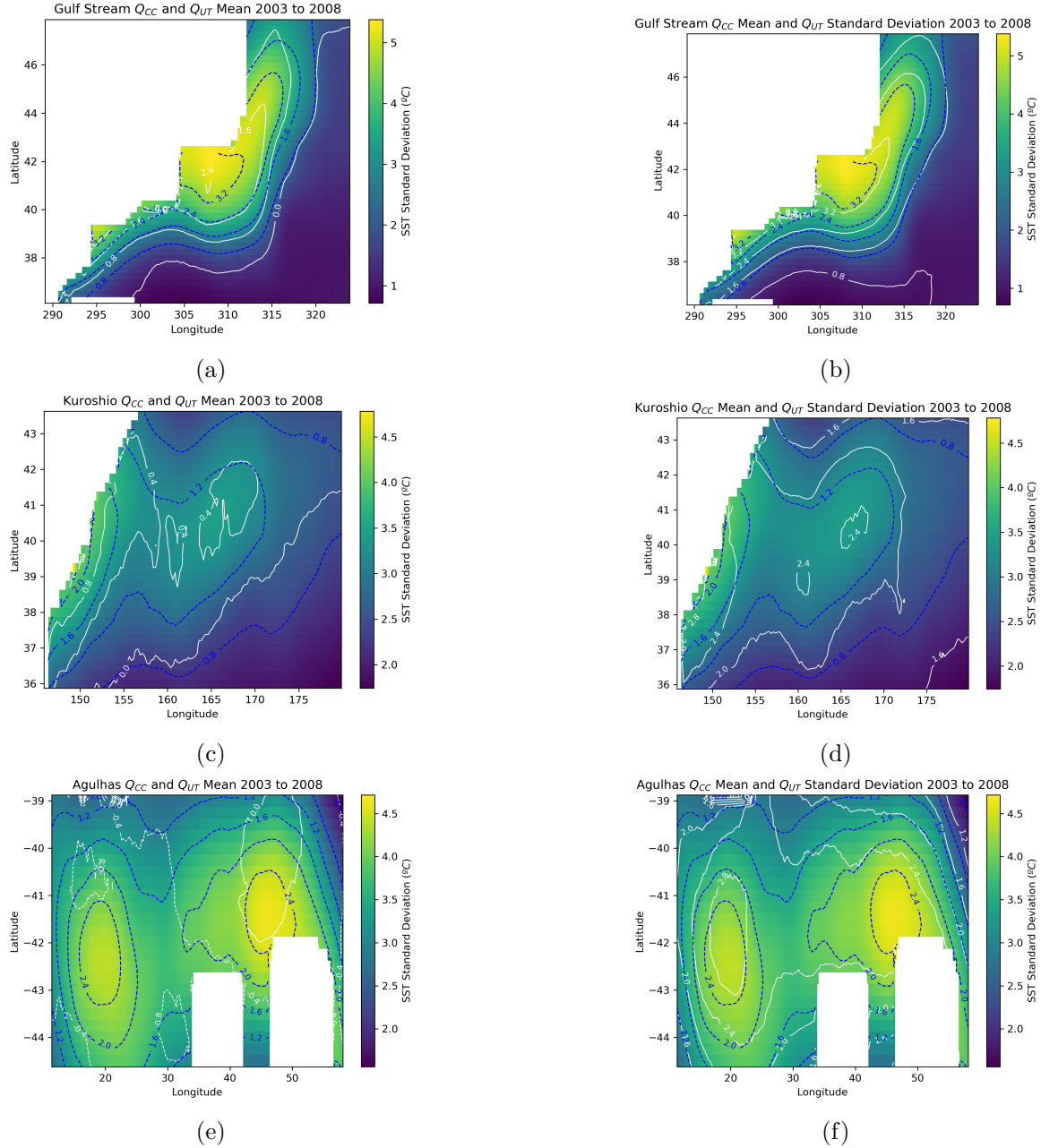


Figure 5: Trial 1. Maps of the temporal average of the rectification in the Gulf Stream (a, b), Kuroshio Extension (c, d), and Agulhas Return Current (e, f) over the entire dataset (1/1/2003 to 12/31/2008). The colors represent the standard deviation of SST to reveal the regions with the greatest ocean mesoscale variability. The blue dashed lines represent the mean rectification from the Clausius Clapeyron term (Q_{CC}) and the white lines either represent the mean rectification from the covariability of wind speed and SST (Q_{UT}) (a, c, e) or the standard deviation of the covariability (b, d, f). The contour spacing is $0.4 W/m^2$ for the Kuroshio Extension and Agulhas Return Current and is $0.8 W/m^2$ for the Gulf Stream.

Figure 5 reveals the spatial distribution of the rectification. We plot both the mean of the covariability term (Figure 5 (a), (c), and (e)) and the standard deviation (Figure 5 (b), (d), and (f)) to account for the covariability term containing both positive and negative values. The standard deviation of the covariability and the Clausius Clapeyron term appear to be spatially correlated. Both are the greatest over regions of large mesoscale variability which we represent using the SST standard deviation.

5.1.1 Seasonal Cycle

Next we seek to understand the cause of the seasonal cycle. Figure 3 reveals a seasonal cycle in the Clausius Clapeyron term (Q_{CC}), however, there is no evident seasonal cycle in the covariability term (Q_{UT}). In Figure 6, we plotted variables of the high rectification region of the Gulf Stream (40.875° N to 43.125° N and 304.625° W to 312.125° W) over the course of one year, 2004. We focused on this region of the Gulf Stream because the rectification is the most prominent. We plotted the daily average of the rectification and various variables that might inform us of the seasonal cycle including: the large scale LHF (Q_0), the Clausius Clapeyron term (Q_{CC}), the covariability of wind speed and SST (Q_{UT}), the low passed SST and wind speed, the standard deviation of SST, the mean and standard deviation of the covariance of wind speed and SST ($\overline{U'T'}$). The results are similar for all three study regions.

The large scale LHF depends on low pass wind speed linearly and low pass SST nonlinearly. This is evident if you recall that the large scale LHF is simply Equation 1 calculated with low pass wind speed and low pass SST, and saturation humidity is nonlinearly related to SST. Thus, you see the impact of both low pass SST and low pass wind speed on the large scale LHF such that it is greater in fall and early winter and smaller in spring and early summer. The derivative term for both the Clausius Clapeyron term and the covariability are calculated with low pass SST and low pass wind speed (see Equation 8). Thus, we predicted the rectification to have a seasonal cycle similar to the large scale LHF, however, that is not the case. The covariability does not exhibit a seasonal cycle. The low pass SST's seasonal cycle is 45° to 90° out of phase with the seasonal cycle of the Clausius Clapeyron term. The seasonal cycle of the Clausius Clapeyron term is directly related to the low pass wind speed, the covariance $\overline{U'T'}$ mean and standard deviation, and the standard deviation of SST. Thus, it is also in phase with these variables.

The covariability term is directly related to the covariance of wind speed and SST ($\overline{U'T'}$). This dependence explains the large daily variability. Synoptic wind variations also likely contribute to the high variability. However, the lack of a seasonal cycle in the covariability term is surprising. Studies have found that the coupling between SST and wind is stronger in the winter than in the summer; the seasonal difference in this coupling can be a factor of five in the Gulf Stream and Kuroshio Extension (Chelton and Xie, 2010; O'Neill et al., 2010). Perhaps the seasonal cycle in the covariability term is interfered with by the low pass SST, which is out of phase with $\overline{U'T'}$. We will investigate this further in the following section.

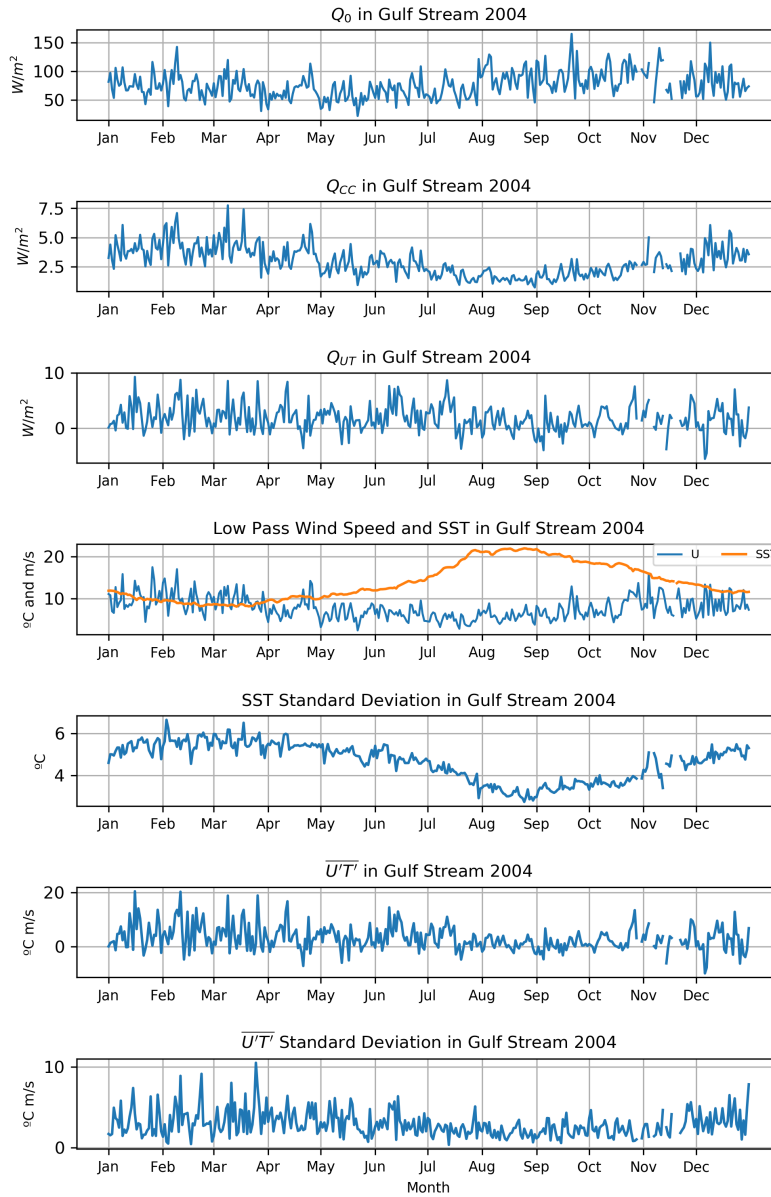


Figure 6: Trial 1. Daily average of the large scale LHF (Q_0), the Clausius Clapeyron term (Q_{CC}), covariability of wind speed and SST (Q_{UT}), low pass SST and wind speed, the standard deviation of SST, $\overline{U'T'}$, and the standard deviation of $\overline{U'T'}$ in the high rectification region of the Gulf Stream (40.875° N to 43.125° N and 304.625° W to 312.125° W) over the course of 2004.

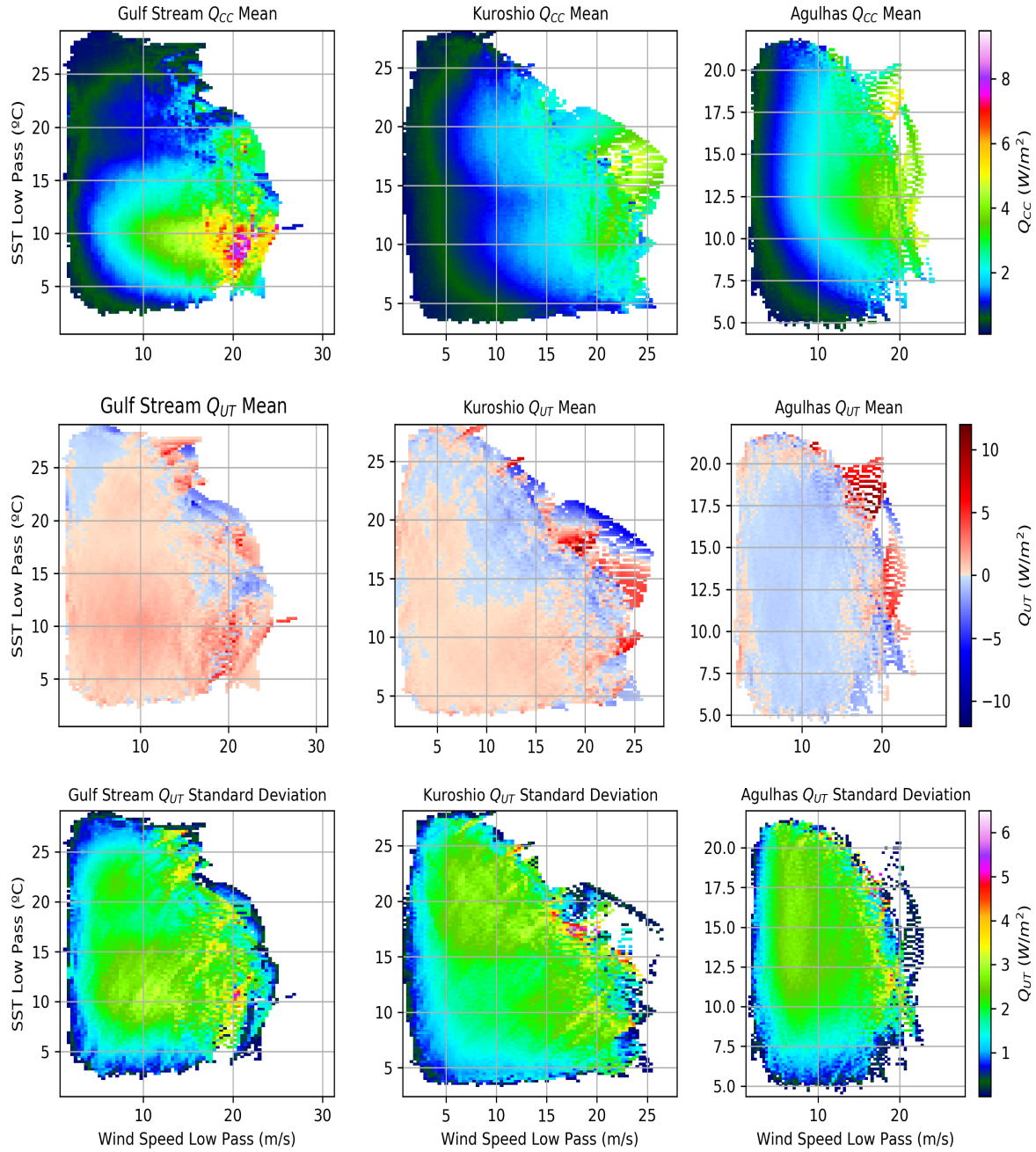


Figure 7: Trial 1. Dependence of the rectification of the Clausius Clapeyron term (Q_{CC}) and the covariability of SST and wind speed (Q_{UT}) on low pass wind speed and low pass SST in the Gulf Stream, Kuroshio Extension, and Agulhas Return Current from 2003-2008. The rectification was isolated each time it occurred within a chosen SST and wind speed. We then found the average of the isolated rectifications (see the top two rows) or the standard deviation (see the bottom row). Only the mean is plotted for Q_{CC} while the mean and standard deviation are both plotted for Q_{UT} .

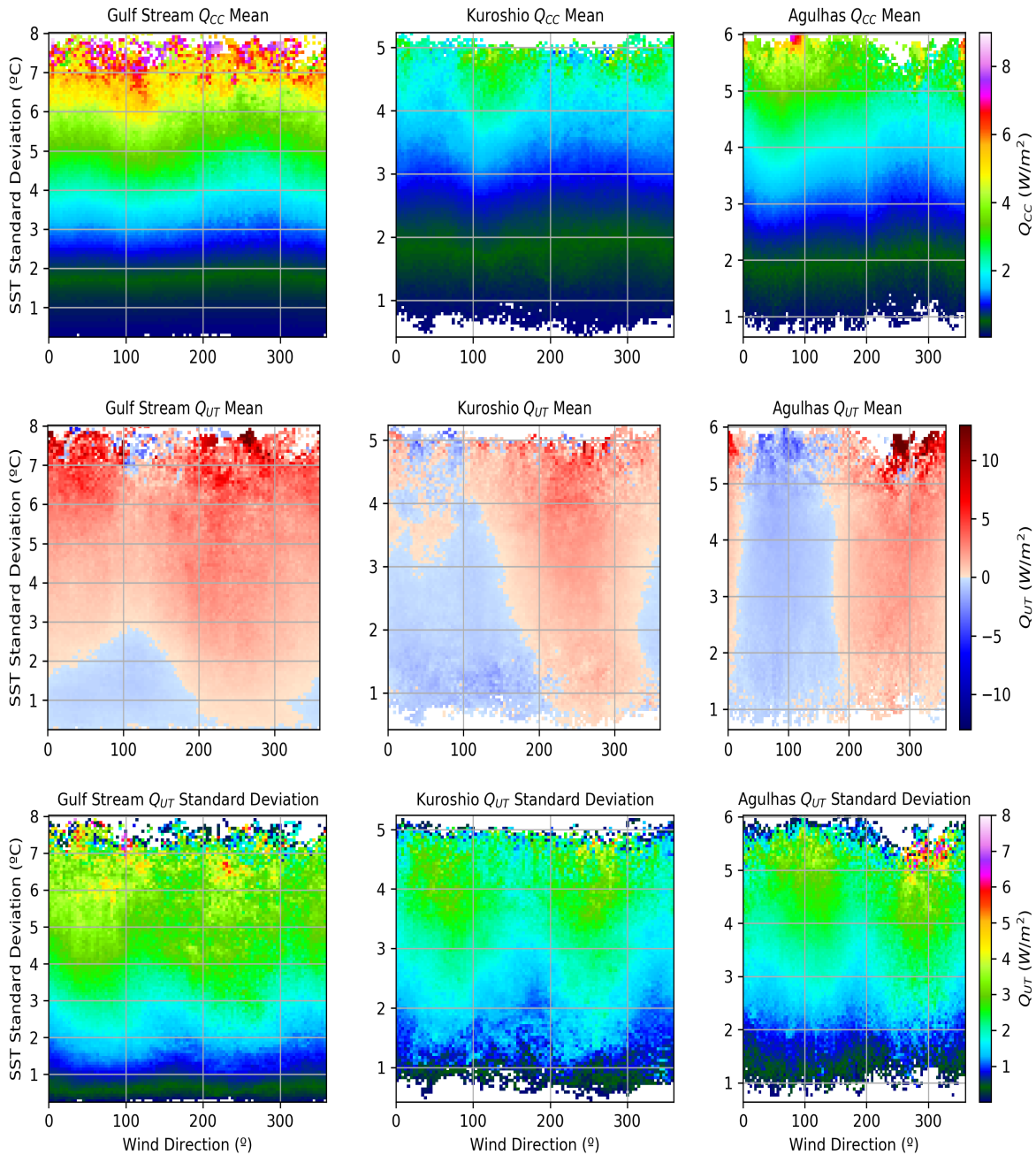


Figure 8: Trial 1. Dependence of the rectification of the Clausius Clapeyron term (Q_{CC}) and the covariability of SST and wind speed (Q_{UT}) on wind direction and the standard deviation of SST in the Gulf Stream, Kuroshio Extension, and Agulhas Return Current from 2003-2008. The rectification was isolated each time it occurred within a chosen SST and wind speed. We then found the average of the isolated rectifications (see the top two rows) or the standard deviation (see the bottom row). Only the mean is plotted for Q_{CC} while the mean and standard deviation are both plotted for Q_{UT} . Zero degrees indicates wind blowing North.

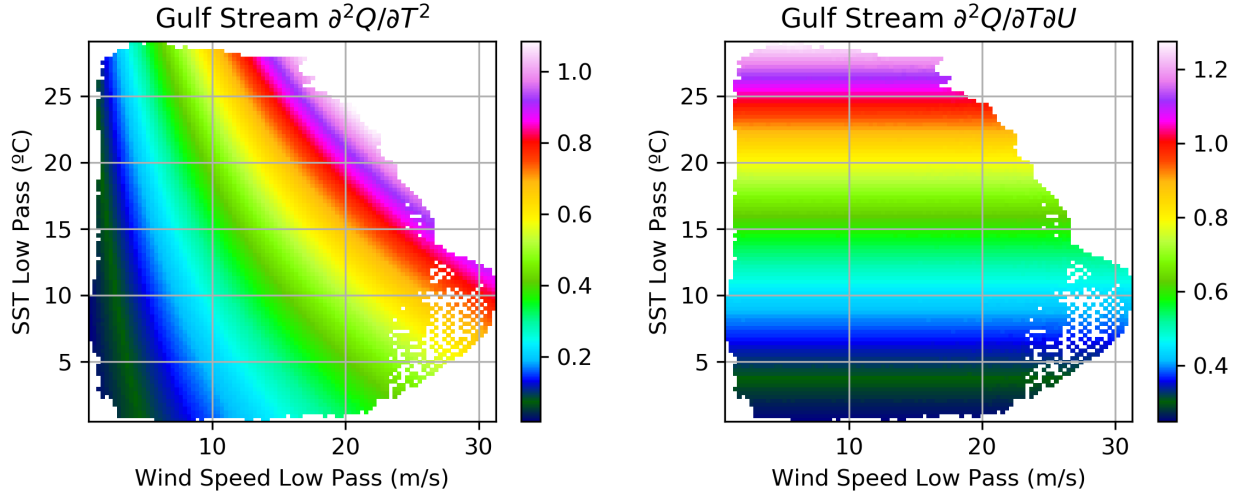


Figure 9: Trial 1. The relationship between the second derivative terms in the Taylor Expansion Equation 8 and low pass SST and low pass wind speed in the Gulf Stream over the entire data period 2003-2008. The left plot is of the second derivative of LHF with respect to SST ($\partial^2 Q / \partial T^2$) and the right plot is the second derivative of LHF with respect to SST and wind speed ($\partial^2 Q / \partial T \partial U$).

5.1.2 Rectification Dependence on Wind and SST

Our results from Figure 6 suggest that the Clausius Clapeyron term is dependent on low pass wind speed as opposed to low pass SST. Meanwhile the covariability does not reveal any obvious dependence on any variables other than its direct relationship to the covariance $\overline{U'T'}$. In this section, we will further explore the dependence the rectification terms have on wind speed and SST utilizing Figure 7 to 10.

First, we will look at the dependence of the rectification terms on background wind speed. Figure 7 reveals that the Clausius Clapeyron term has a strong dependence on background wind speed such that larger wind speed is associated with larger rectification. However, there is no evident relationship between background wind speed and the covariability term. The most positive and most negative covariability means generally occur in the largest background wind speeds (> 15 m/s), however, there is no clear structure for the lower wind speeds. The reasoning for this becomes clear if you reference Figure 9. The Clausius Clapeyron term contains $\partial^2 Q / \partial T^2$, which directly relates to background wind speed. Meanwhile, the covariability term depends on $\partial^2 Q / \partial T \partial U$, which is independent of background wind speed (see Equation 8 and Figure 9).

Next, we will look at the dependence of the rectification terms on SST. The rectification terms appear to be independent of background SST based on Figure 7. However, from Figure 9, we know that $\partial^2 Q / \partial T \partial U$ from the covariability term is directly related to background SST. Thus, there must be something interfering with this relationship in the covariability term to hide relationship in Figure 7. Indeed we confirm that the covariance $\overline{U'T'}$ is greatest

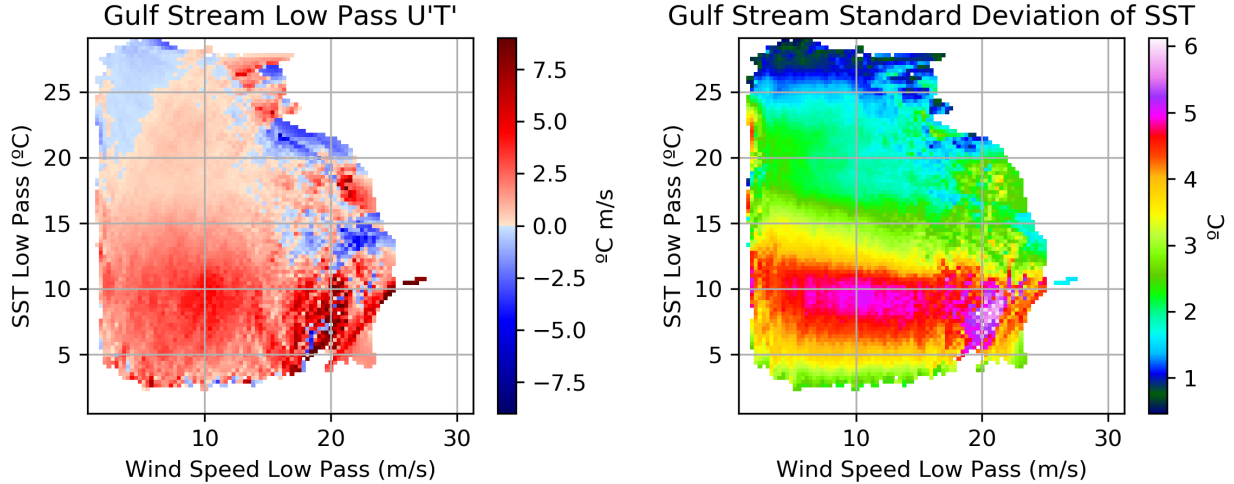


Figure 10: Trial 1. The left plot is the average value of $\overline{U'T'}$ at each low pass wind speed and low pass SST. The right plot is the average of the standard deviation of SST at each low pass wind speed and low pass SST. Both plots are of all data in the Gulf Stream over all time. Note that for the left plot, values of $\overline{U'T'}$ actually reach up to 16 $^{\circ}\text{C m/s}$, however, the range plotted was limited so that the structure in the lower values was visible.

in times of low background SST in Figure 10. Figure 9 reveals that $\partial^2 Q / \partial T^2$ from the Clausius Clapeyron term has a very slight relationship to low pass SST. $\partial^2 Q / \partial T^2$ slightly increases with SST at low wind speeds (< 10 m/s), but greatly increases with SST at high wind speeds (> 15 m/s).

Figure 8 and 10 reveal the dependence on the standard deviation of SST. We can use it as a proxy to represent ocean mesoscale activity. The Clausius Clapeyron term appears to be independent of wind direction, yet directly relates to the standard deviation of SST, which we anticipated. The covariability term does not have an obvious dependence on the SST standard deviation if you only look at the mean of the covariability term, however, the standard deviation of the covariability reveals that there is a dependence on SST standard deviation. This dependence suggests that in times of large mesoscale ocean variability, the magnitude of the covariability term is also large; however, the covariability term will not necessarily be positive or negative depending on the SST standard deviation. From Figure 10, the standard deviation of SST depends on background SST. The standard deviation of SST peaks in a background SST of 6 to 13 $^{\circ}\text{C}$ in the Gulf Stream, and it is the smallest in background SST of 25 $^{\circ}\text{C}$ and greater. These features are very similar for the other regions except that the standard deviation of SST is the greatest in the Agulhas Return Current at a background SST of 8 to 16 $^{\circ}\text{C}$. The Kuroshio Extension more closely resembles the Gulf Stream, except that there are some large values of SST standard deviation at a background SST of 15 to 20 $^{\circ}\text{C}$. This explains the features that we see in the Clausius Clapeyron term in Figure 7.

In Figure 8, we study the relationship between the rectification and wind direction. Wind

from the poles will be cooler and drier. Wind blown from landmass will be warmer in the summer months and cooler in the winter months compared to the surrounding ocean. We hypothesize this will impact the rectification of latent heat flux. The Clausius Clapeyron term appears to be independent of wind direction, however, wind direction does have an impact on the covariability term. The plot of the covariability’s standard deviation reveals that the magnitude of the covariability term is slightly greater when the wind blows northeast (45°) and southwest (225°) in the Gulf Stream and Kuroshio Extension. In the Agulhas Return Current, the magnitude is greater when blowing in a southeastern (135°) or westward (270°) direction. However, the mean covariability is negative when the wind blows northeast, east, or southeast (45° to 135°) and positive when the wind blows South West, West, and northwest (225° to 315°).

After exploring the variable dependence of the rectification, we can hypothesize the drivers of the seasonal cycle. The seasonal cycle of the Clausius Clapeyron term is driven by both the standard deviation of SST and the background wind speed. The covariability term exhibits no seasonal cycle because it depends on both the background SST and $\overline{U'T'}$, which are out of phase with one another.

5.1.3 Filter Size Dependence

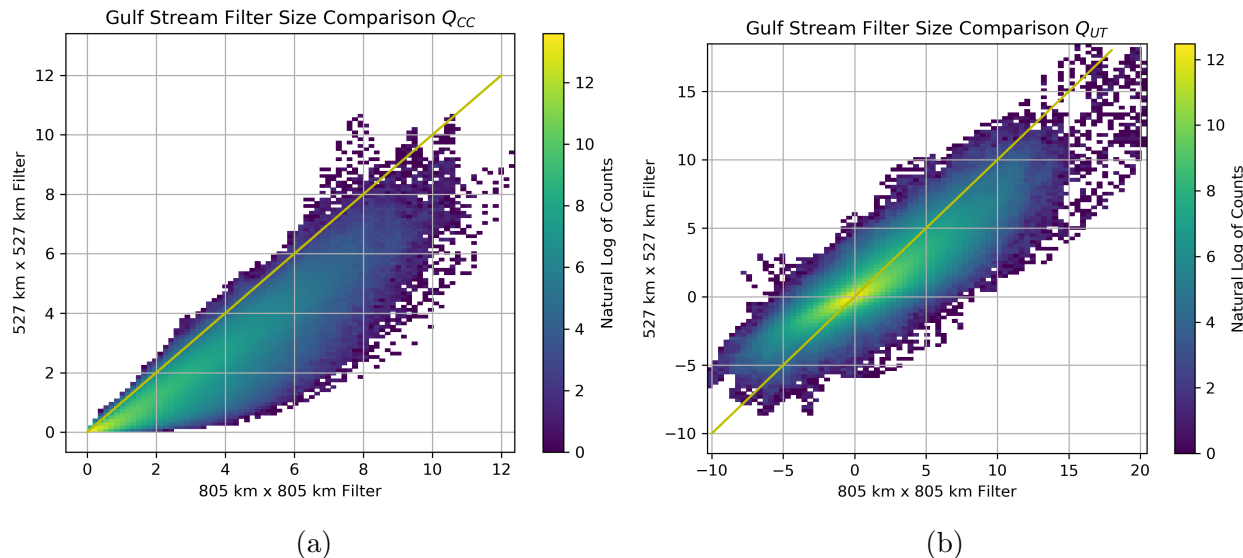


Figure 11: Trial 1. Two-dimensional probability density function (PDF) of (a) the Clausius Clapeyron term (Q_{CC}) and (b) the covariability of wind speed and SST (Q_{UT}). The colors of the bins show the log base 10 of the number of times the rectification occurs within a certain W/m^2 for both filter sizes. The y-axis is the rectification calculated with a filter size of 527 km and the x-axis is the rectification calculated with a filter size of 805 km in the Gulf Stream from 2003-2008. The yellow line is linear and has a slope of 1.

In Section 4.4, we discussed our decision to chose a 805 km filter size. All of the results

presented in this study are for the 805 km filter size. However, the results do depend on the filter size, thus, it is useful to explore the effect of different filter sizes. As the filter size increases, the SST anomalies and wind speed anomalies increase in size. This causes an increase in the size of the Clausius Clapeyron term with an increase in filter size (see Table 2 and Figure 11). In Figure 11, the bins under the yellow line are instances when the larger 805 km filter size results in larger rectification compared to the smaller 527 km filter size. As expected, the Clausius Clapeyron term increases with increasing filter size more than 80% of the time.

For the covariability term, there are many instances where the increase in filter size decreases the covariability as well as increases the covariability term. For example, the increase in filter size from a 527 km to a 805 km filter decreases the mean of the covariability term by $0.099 W/m^2$ in the Gulf Stream (see Table 2). However, in the Kuroshio Extension and the Agulhas Return Current, the same increase in filter size actually decreases the covariability term. When our covariability term is positive, that indicates that we have captured a majority of mesoscale features with our filter size because mesoscale SST and wind speed are positively correlated at the mesoscale and negatively correlated at the large-scale (Small et al., 2008; Chelton and Xie, 2010). Mesoscale features change sizes depending on latitude, so it is not surprising that the covariability term depends on both the region and filter size (Laurindo et al., 2019).

Filter Size	Gulf Stream (W/m^2)	Kuroshio (W/m^2)	Agulhas (W/m^2)
305 km Q_{CC}	0.455	0.157	0.211
305 km Q_{UT}	0.409	0.084	0.100
527 km Q_{CC}	0.807	0.341	0.468
527 km Q_{UT}	0.554	0.068	0.026
805 km Q_{CC}	1.149	0.639	0.870
805 km Q_{UT}	0.455	-0.021	-0.257
971 km Q_{CC}	1.333	0.869	1.146
971 km Q_{UT}	0.284	-0.097	-0.505

Table 2: Trial 1. The mean of the Clausius Clapeyron term (Q_{CC}) and the covariability of wind speed and SST (Q_{UT}) when the filtering is conducted at each particular filter size. The mean of entire dataset is taken for Q_{CC} and Q_{UT} for four top hat filter sizes in the Gulf Stream, Kuroshio Extension, and Agulhas Return Current.

5.1.4 ε

We calculate ε in our Taylor Expansion Equation 8 by $\varepsilon = Q_0 - Q_1 - Q_{CC} - Q_{UT}$. ε encapsulates the higher order terms of the Taylor Expansion and any error in our calculations. Table 3 and Figure 12 reveals that ε is at least an order of 10 smaller than both of our rectification terms Q_{CC} and Q_{UT} , thus we conclude that our Taylor Expansion works. It encompasses all of the important nonlinearities in the LHF.

	Gulf Stream (W/m^2)	Kuroshio (W/m^2)	Agulhas (W/m^2)
ε mean	-0.07	0.00	0.02
ε max (95th%)	2.54 (0.18)	1.12 (0.16)	1.86 (0.28)
ε min (5th%)	-3.07 (-0.50)	-0.95 (-0.16)	-1.13 (-0.21)

Table 3: Trial 1. Mean, maximum and 95th percentile, minimum and 5th percentile of ε across the entire data period in the Gulf Stream, Kuroshio Extension, and Agulhas Return Current.

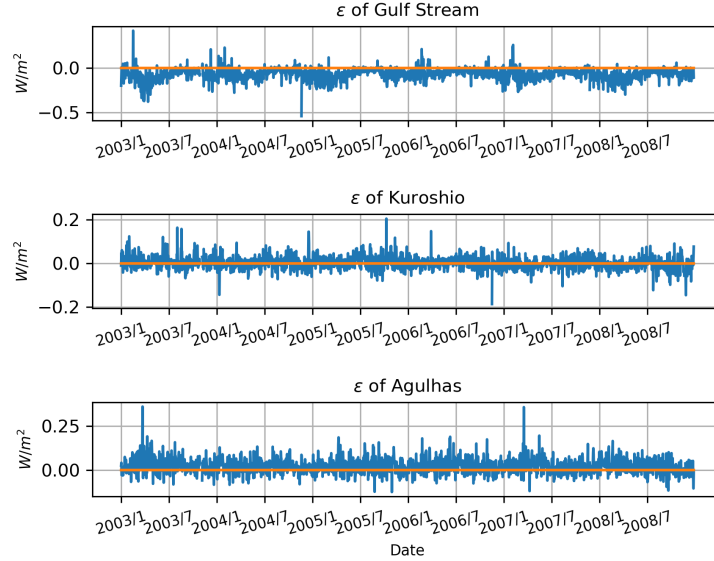


Figure 12: Trial 1. Daily average of ε in the Gulf Stream, Agulhas Return Current, and Kuroshio Extension with satellite data. The orange line is zero.

5.2 Trial 2: Reanalysis Data

For Trial 2, we will utilize ERA5 reanalysis data in the Taylor Expansion Equation 7 for the same three regions and time period as Trial 1. The immediate difference from Trial 1, is that we have data for specific humidity in Trial 2. In Trial 1, the specific humidity we used depended on SST, but now specific humidity becomes an independent variable which adds another nonlinear term to our Taylor Expansion: the covariability of specific humidity and wind speed (Q_{UH}).

We look to Figure 13 to Figure 16, and Table 4 to quantify the rectification terms. On average, the Clausius Clapeyron term is about 0.78 to 1.36 W/m^2 , the covariability of wind speed and SST is -0.47 to 0.73 W/m^2 , and the covariability of wind speed and specific humidity is -0.68 to 0.61 W/m^2 , depending on the region. Similar to Trial 1, the mean of the Clausius Clapeyron term is greater than both covariability terms; however, the range of the

	Gulf Stream (W/m^2)	Kuroshio (W/m^2)	Agulhas (W/m^2)
Q_0 mean	101.38	70.14	74.26
Q_0 max (95th%)	555.29 (236.81)	418.89 (178.65)	418.02 (177.98)
Q_0 min (5th%)	-111.20 (14.48)	-101.81 (-3.37)	-88.13 (1.62)
Q_{CC} mean	1.08	0.78	1.36
Q_{CC} max (95th%)	11.41 (3.74)	4.73 (1.60)	5.92 (2.57)
Q_{CC} min (5th%)	0.00 (0.05)	0.02 (0.26)	0.01 (0.49)
Q_{UT} mean	0.73	-0.47	-2.55
Q_{UT} max (95th%)	59.80 (14.19)	33.65 (10.13)	42.83 (10.91)
Q_{UT} min (5th%)	-45.53 (-9.74)	-34.04 (-10.65)	-42.90 (-14.92)
Q_{UH} mean	-0.68	-0.22	0.61
Q_{UH} max (95th%)	39.40 (7.67)	40.82 (6.71)	45.02 (7.91)
Q_{UH} min (5th%)	-55.42 (-9.30)	-36.91 (-7.19)	-37.99 (-6.92)

Table 4: Trial 2. Mean, maximum and 95th percentile, minimum and 5th percentile of the large scale LHF (Q_0), the Clausius Clapeyron term (Q_{CC}), the covariability of wind speed and SST (Q_{UT}), and the covariability of wind speed and specific humidity (Q_{UH}) across the entire data set. Values are provided for the Gulf Stream, Kuroshio, and Agulhas Return Current.

covariability term exceeds the range of the Clausius Clapeyron term. From the 5th and 95th percentile the Clausius Clapeyron term ranges from 0.05 to 3.74 W/m^2 , the covariability of wind speed and SST ranges from -14.92 to 14.19 W/m^2 , and the the covariability of wind speed and specific humidity ranges from -9.30 to 7.91 W/m^2 .

Figure 17 reveals the spatial distribution of the rectification. We plotted the mean of the Clausius Clapeyron term and the mean and standard deviation of both covariability terms. Similar to Trial 1, the standard deviation of the covariability of wind speed and SST and the Clausius Clapeyron term appear to be spatially correlated. Both are the greatest over regions of large mesoscale variability which we represent using the SST standard deviation. However, the covariability of wind speed and specific humidity is not spatially correlated with the SST standard deviation or the other rectification terms.

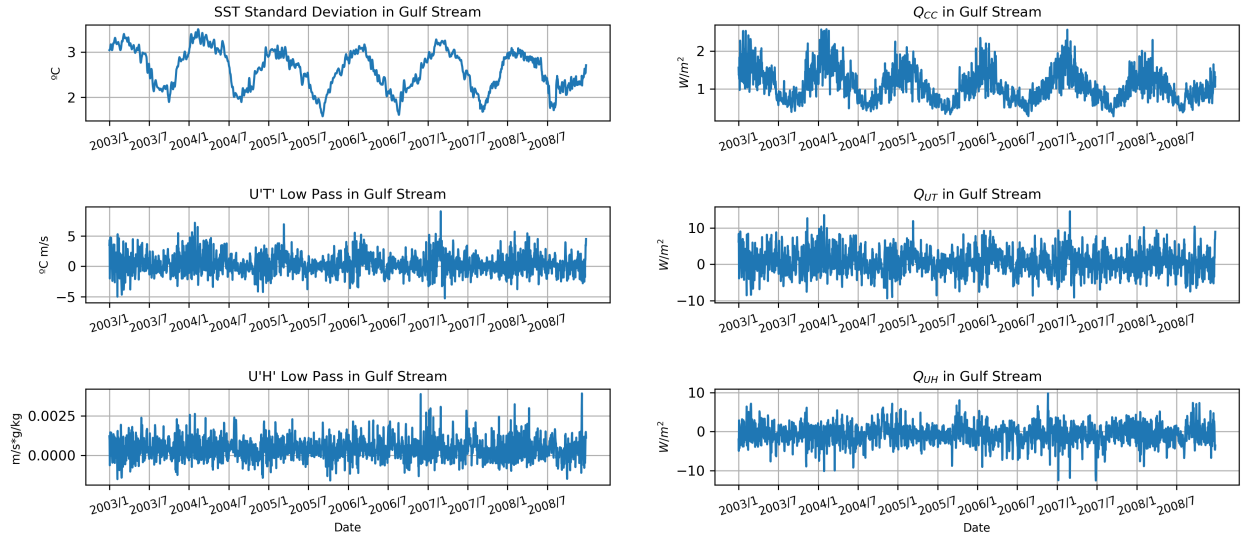


Figure 13: Trial 2. Daily and spatial average of the SST standard deviation, covariance $\overline{U'T'}$, covariance $\overline{U'H'}$, the Clausius Clapeyron term (Q_{CC}), the covariability of wind speed and SST (Q_{UT}), and the covariability of wind speed and specific humidity (Q_{UH}) in the Gulf Stream.

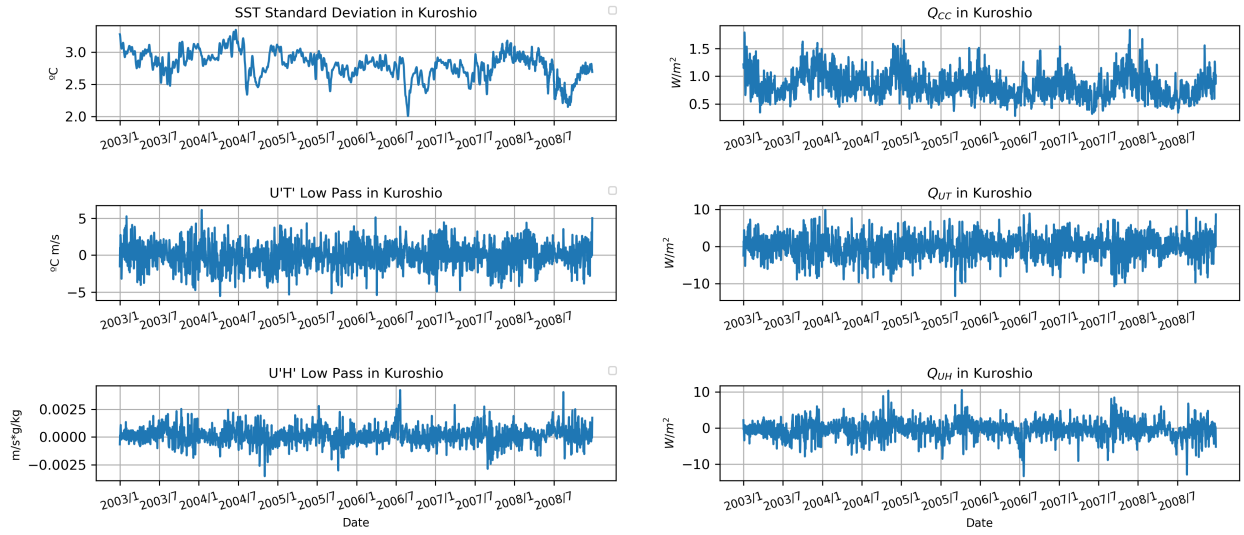


Figure 14: Trial 2. Daily and spatial average of the SST standard deviation, covariance $\overline{U'T'}$, covariance $\overline{U'H'}$, the Clausius Clapeyron term (Q_{CC}), the covariability of wind speed and SST (Q_{UT}), and the covariability of wind speed and specific humidity (Q_{UH}) in the Kuroshio Extension.

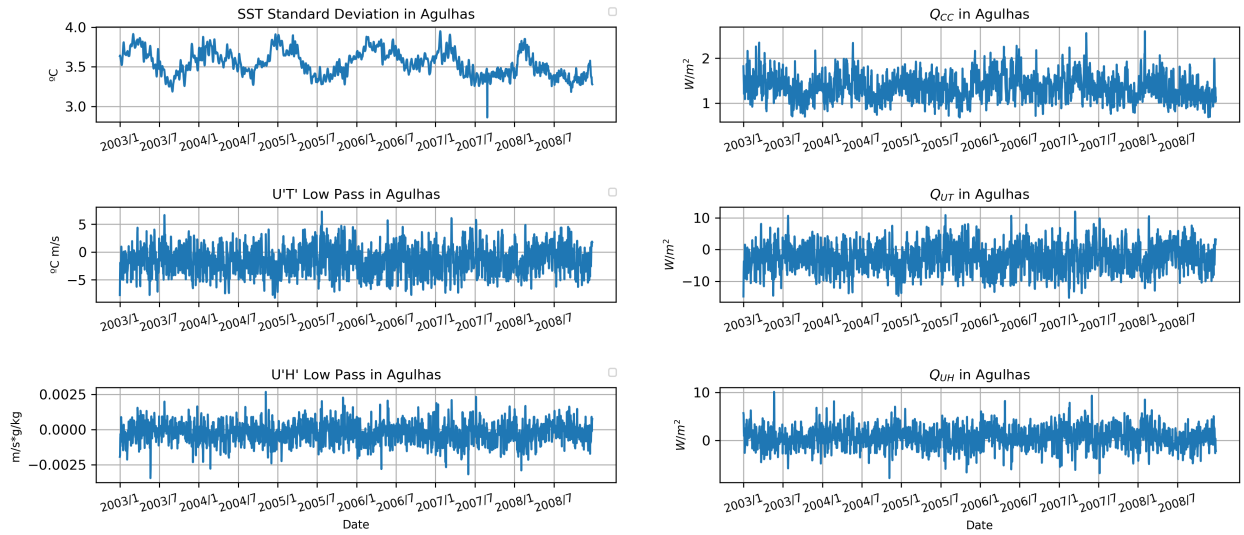


Figure 15: Trial 2. Daily and spatial average of the SST standard deviation, covariance $\overline{U'T'}$, covariance $\overline{U'H'}$, the Clausius Clapeyron term (Q_{CC}), the covariability of wind speed and SST (Q_{UT}), and the covariability of wind speed and specific humidity (Q_{UH}) in the Agulhas Return Current.

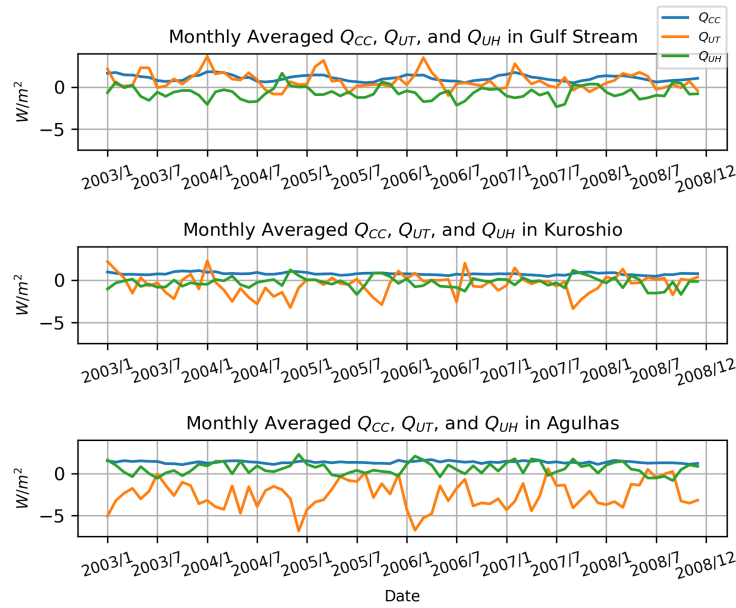


Figure 16: Trial 2. Monthly and spatial average of the Clausius Clapeyron term (Q_{CC}) in blue, the covariability of wind speed and SST (Q_{UT}) in orange, and the covariability of wind speed and specific humidity (Q_{UH}) in green in the Gulf Stream, Agulhas Return Current, and Kuroshio Extension.

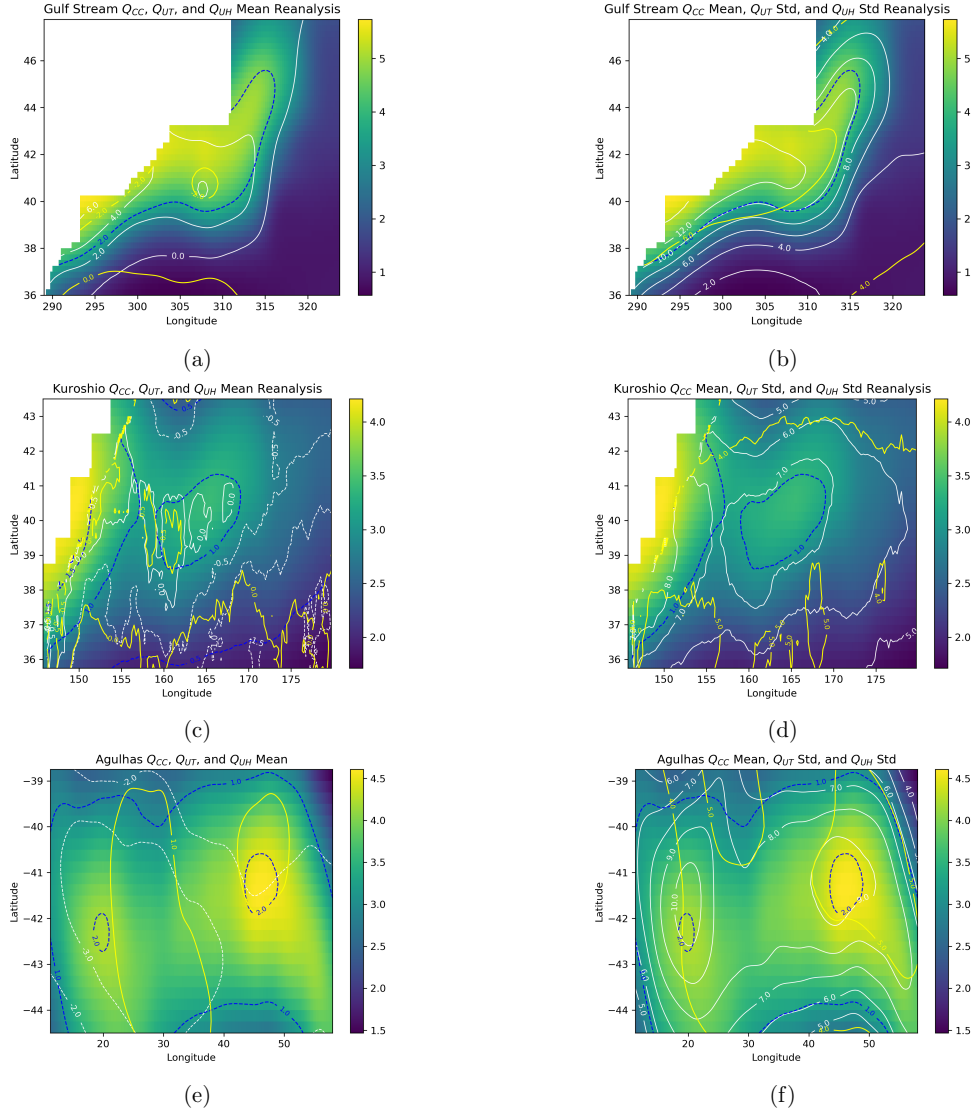


Figure 17: Trial 2. Map of the temporal average of the rectification in the Gulf Stream (a, b), Kuroshio Extension (c, d), and Agulhas Return Current (e, f) over the entire dataset (1/1/2003 to 12/31/2008). The colors represent the standard deviation of SST in order to reveal the regions with the greatest ocean mesoscale variability. The blue dashed lines represent the mean rectification from the Clausius Clapeyron term (Q_{CC}). The white lines represent the mean rectification from the covariability of wind speed and SST (Q_{UT}) in plots (a), (c), and (e) and the standard deviation of the covariability in plots (b), (d), and (f). The yellow lines represent the mean rectification from the covariability of wind speed and specific humidity (Q_{UH}) in plots (a), (c), and (e) and the standard deviation of the covariability in plots (b), (d), and (f). Contours are spaced by $2 W/m^2$ for (a) and (b), $1 W/m^2$ for plots (d), (e), and (f), and $0.5 W/m^2$ for plot (c).

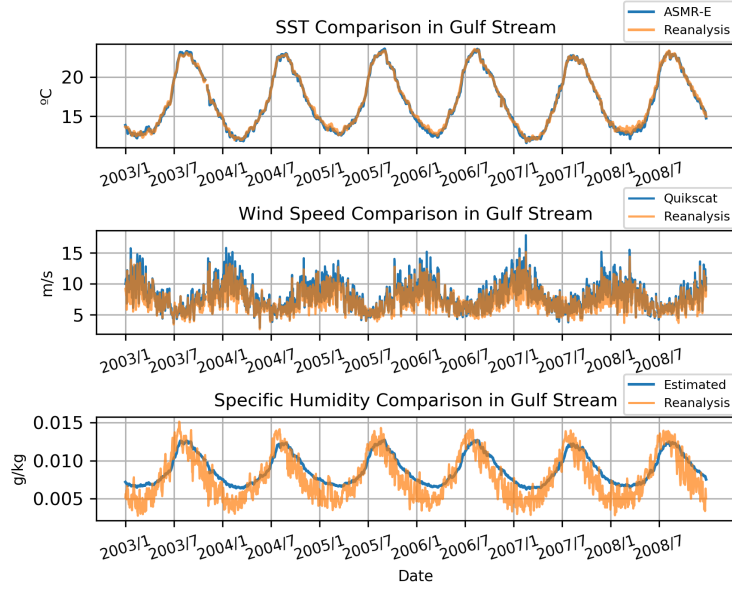


Figure 18: Trial 1 and Trail 2. Comparison of the daily average of reanalysis and satellite data used in Trial 1 and Trial 2. ERA5 Reanalysis data is in orange and satellite data is in blue. SST, wind speed, and specific humidity in the Gulf Stream from 2003 to 2008. We ensured that data from the same location and time were compared by removing the data present in one dataset that was absent in the other.

5.2.1 Trial 1 and Trial 2 Comparison

In our preliminary results, it is obvious that the reanalysis data in Trial 2 has produced results that differ greatly from the satellite data in Trial 1. The Clausius Clapeyron term calculated from the reanalysis data is smaller than the satellite data by an average of $0.07 W/m^2$ in the Gulf Stream, $0.26 W/m^2$ in the Kuroshio Extension, and $0.43 W/m^2$ in the Agulhas Return Current. For the mean of the covariability of SST and wind speed, Trial 1 is less than Trial 2 by $0.27 W/m^2$ in the Gulf Stream. Trial 1 exceeds Trial 2 by $0.66 W/m^2$ in the Kuroshio Extension and $2.15 W/m^2$ in the Agulhas Return Current. For the covariability of wind speed and SST, the reanalysis data spans a much larger range compared to the satellite data. From the 5th to the 95th percentile, Trial 1 spans about $7 W/m^2$ and Trial 2 spans about $24 W/m^2$, with slight differences in each region.

One obvious cause for the difference in results from Trial 1 to Trial 2, is that they have different coverage. Although we study the same region and time period, there are large gaps in the satellite data. The other differences are due to the dissimilarities in the wind speed, SST, and specific humidity in Trial 1 and Trial 2 (Figure 18). We have already done an analysis of the dependence of the rectification on these variables, therefore, if we understand how these variables differ from Trial 1 to Trial 2, it may reveal why the rectification differs. In order to compare the variables in Figure 18, we ensured that data from the same location

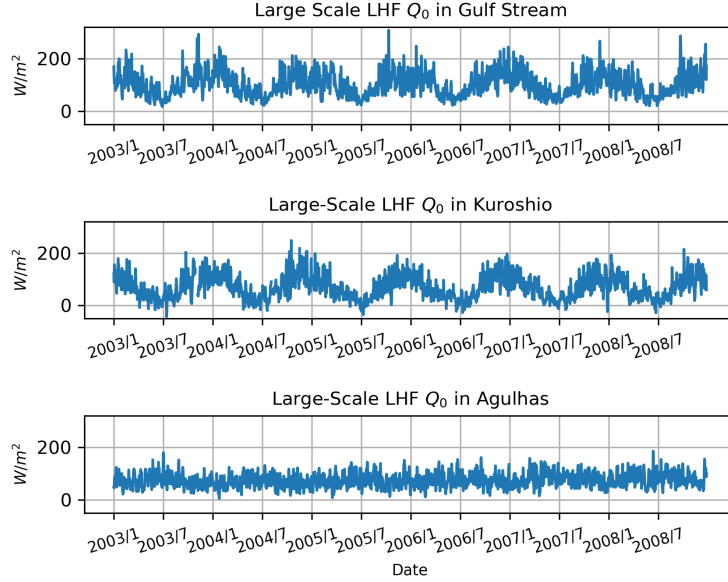


Figure 19: Trial 2. Daily and spatial average of large-scale LHF (Q_0) in the Gulf Stream, Agulhas Return Current, and Kuroshio Extension.

and time were compared by removing the data present in one dataset that was absent in the other. The difference between the wind speed, SST, and specific humidity is very similar in all three of our study regions, thus we only show the Gulf Stream in Figure 18.

The daily average of SST is very similar from ASMRE to the reanalysis, thus saturation humidity will also be very similar between to the two trials because it was calculated from SST. Other studies show that the ERA5 SST in the Kuroshio Extension and Gulf Stream differed from observational data by a small fraction of a K as mentioned in Sroka et al. (2022). The daily wind speed from each dataset share similar variability, however, the reanalysis wind speed is generally 1-2 m/s slower than the Quikscat wind speed. This decrease in wind speed explains why the Clausius Clapeyron term is lower in the reanalysis trial. The specific humidity from the reanalysis has 0.0005 to 0.002 g/kg daily variability compared to < 0.00005 g/kg for the one we calculated in the satellite trial. In the Gulf Stream and Kuroshio Extension, the seasonal cycle of the specific humidity has a greater range by about 0.07 g/kg for the reanalysis data compared to the satellite data (recall Figure 1). However, this information does not reveal why the covariability of wind speed and SST differs.

5.2.2 Seasonal Cycle

As expected, the seasonal cycle for the Clausius Clapeyron term and the covariability of SST and wind speed resembles the results from Trial 1. There is a seasonal cycle in the Clausius Clapeyron term (Q_{CC}) that ranges from about $2 W/m^2$ in the Gulf Stream, $1 W/m^2$ in the Kuroshio Extension and Agulhas Return Current. However, there is no evident seasonal cycle in either covariability terms.

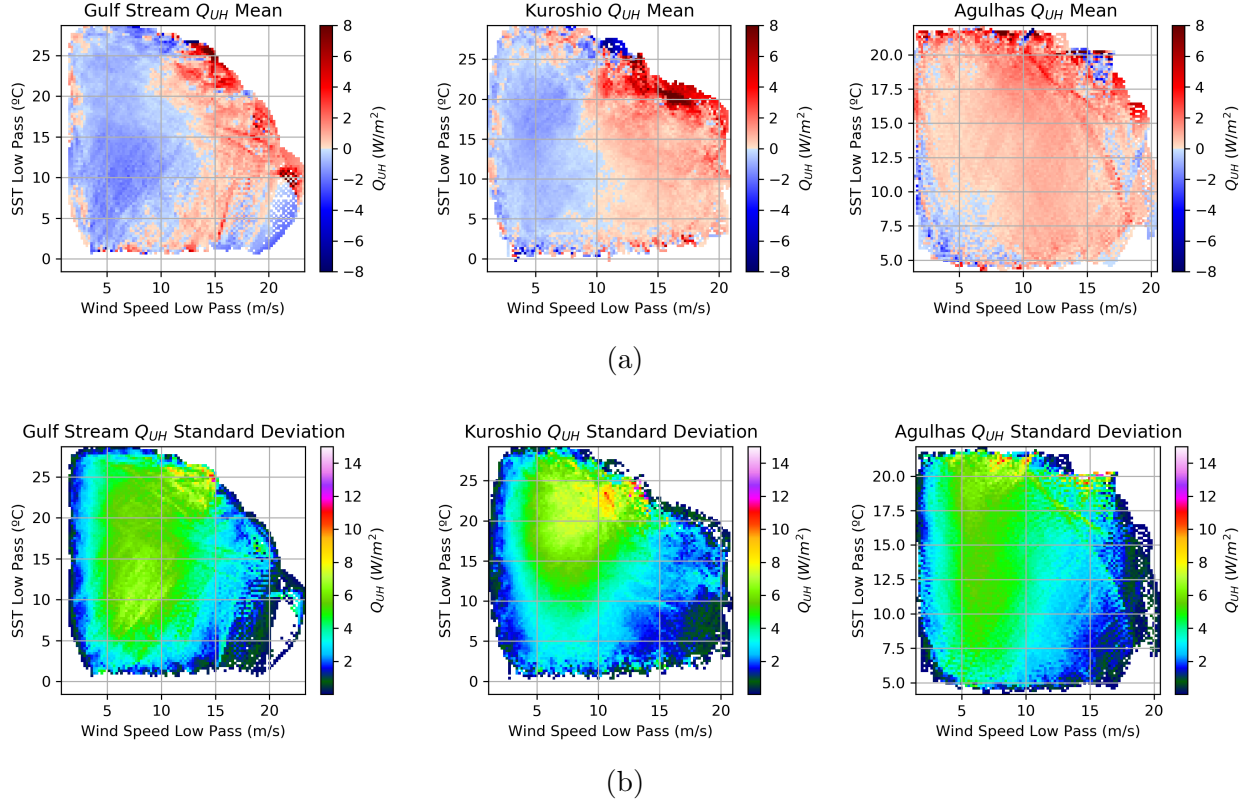


Figure 20: Trial 2. Dependence of the rectification of the covariability of wind speed and specific humidity (Q_{UH}) on background SST and background wind speed in the Gulf Stream, Kuroshio Extension, and Agulhas Return Current from 2003-2008. We took the mean (a) or standard deviation (b) of the rectification within each chosen SST and wind speed.

5.2.3 Rectification Dependence on Wind, SST, and Humidity

The dependence the Clausius Clapeyron term and the covariability of SST and wind speed have on SST and wind speed are the same as Trial 1 because their mathematic relation to SST and wind speed have not changed. In Figure 20, we explored the relationship between the covariability of wind speed and specific humidity and background wind speed and background SST. We suspected that the covariability of wind speed and specific humidity will not have any dependence on the background SST or wind speed because the second derivative term $\partial^2 Q / \partial q_a \partial T$ is a constant. The covariability term is simply $\overline{U'q'_a}$ multiplied by a negative constant. In the Gulf Stream and Kuroshio Extension, the mean covariability is positive in wind speeds greater than 12 m/s, and negative in lower wind speeds. The mean covariability is also greatest when both the background SST and background wind speed are large (> 10 m/s and > 20 °C). The standard deviation of the covariability is independent of background SST; however, it varies with wind speed such that it is greatest in moderate wind speeds (6 to 12 m/s) and it is smaller in very large and very small wind speeds.

Now that specific humidity is an independent variable, we can also look at the dependence

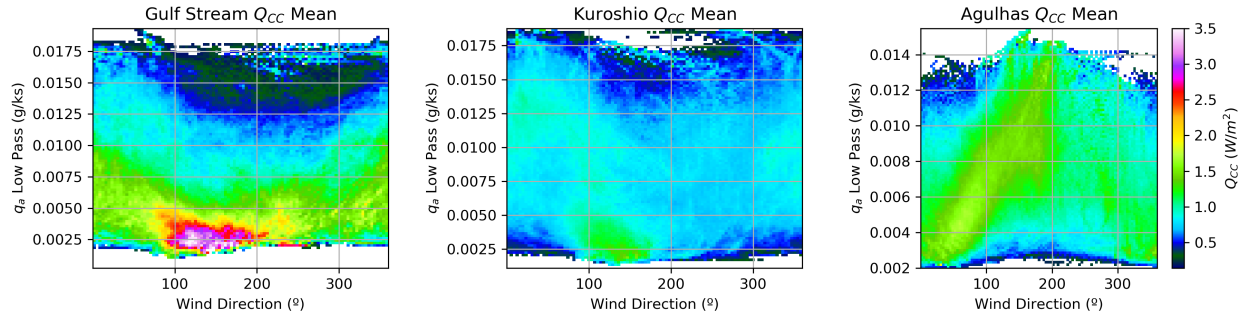


Figure 21: Trial 2. Dependence of the rectification of the Clausius Clapeyron term (Q_{CC}) on background SST and background wind direction in the Gulf Stream, Kuroshio Extension, and Agulhas Return Current from 2003-2008. We took the mean of the rectification within each chosen SST and wind direction. Zero degrees indicates wind blowing North.

of the rectification terms on specific humidity. Figure 21 to 23 reveals a weak relationship between the rectification terms and the specific humidity. In the Gulf Stream, the Clausius Clapeyron term and the covariability of wind speed and SST are largest in low background specific humidity and decrease as the humidity increases. For the covariability of wind speed and SST in the Kuroshio Extension and Agulhas Return Current, you can see this relationship with smaller specific humidity increasing the rectification (Figure 22). However, these seem to be the exception, in all other instances the rectification is the greatest in moderate background specific humidity as opposed to a largest 5% or smallest 5% background specific humidity.

From Figure 21 to 23, we see that the Clausius Clapeyron term is independent of wind direction, however, both covariability terms exhibit a strong dependence on wind direction similar to Trial 1. The mean of the covariability of wind speed and SST is negative in a southeastern (135°) and northward (0°) wind and positive in a southwestern (225°), westward (270°), and northeastern (45°) wind. Surprisingly, the relationship between the wind direction and the covariability of wind speed and specific humidity is, in some ways, opposite to the relationship between wind direction and the covariability of wind speed and SST. In the Gulf Stream and the Kuroshio Extension, the mean of the covariability of wind speed and specific humidity is positive in southeastern (135°) and southern (180°) wind and negative in all other wind. In the Agulhas Return Current the mean is positive in northward to eastward wind ($0^\circ - 90^\circ$) and negative in all other wind. For both covariability terms, their standard deviation is largest in southeastern (135°) or westward (270°) wind.

Cold air outbreaks could potentially impact the rectification. Cold air outbreaks occur in the winter months in the Gulf Stream and Kuroshio, lasting 1-2 days at a time (Shaman et al., 2010; Bond and Cronin, 2008). They are characterized by cold dry air blowing from land in the winter in high latitudes. We look at the Gulf Stream and Kuroshio Extension in Figure 21 to 23 for evidence of cold air outbreaks driving increased rectification. Dry (specific humidity < 0.0050), southeastern wind (135°) increases the Clausius Clapeyron term, especially in the

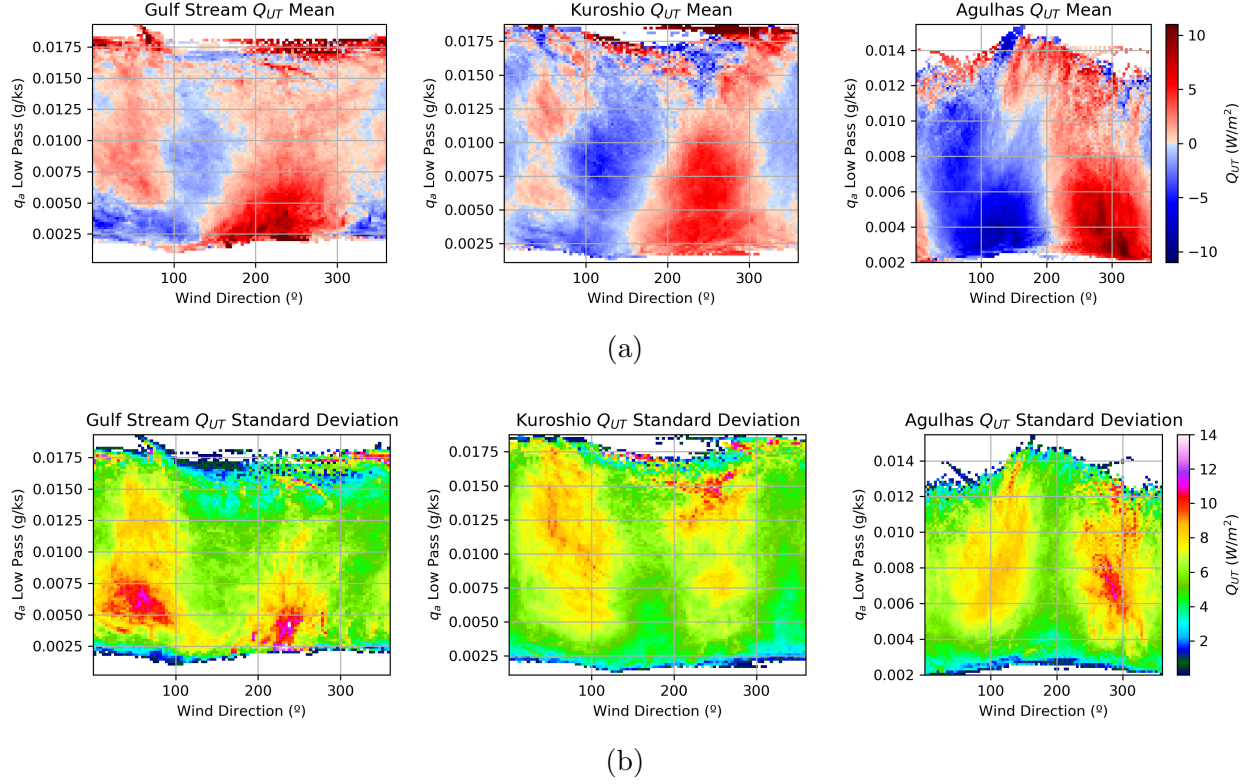


Figure 22: Trial 2. Dependence of the rectification of the covariability of wind speed and SST (Q_{UT}) on background SST and background wind direction in the Gulf Stream, Kuroshio Extension, and Agulhas Return Current from 2003-2008. We took the mean (a) or standard deviation (b) of the rectification within each chosen SST and wind direction. Zero degrees indicates wind blowing North.

Gulf Stream where the average of the Clausius Clapeyron term reaches upwards of $3.5 W/m^2$. However, neither covariability terms visibly increase under these conditions. In addition, this increase in the Clausius Clapeyron term has possibly occurred in seasons other than winter. Cold air outbreaks can also result in large LHF and SHF events. In (Shaman et al., 2010), they found that LHF events that exceed $250 W/m^2$ in the Gulf Stream usually indicates synoptic storms and cold air outbreaks. However, our results found that events of large rectification are not correlated to events of increased large-scale LHF. Currently, we have no evidence that cold air outbreaks drive large rectification events.

5.2.4 ε

ε , which encompasses the higher order terms and the residual, is the same order of magnitude as the rectification terms. The mean ranges from 2.33 to $4.11 W/m^2$ and 90% of its values range from 0.15 to $10.64 W/m^2$ (see Table 5). ε also exhibits a strong seasonal cycle such that it is smaller in summer and larger in winter (see Figure 25). Such a large ε

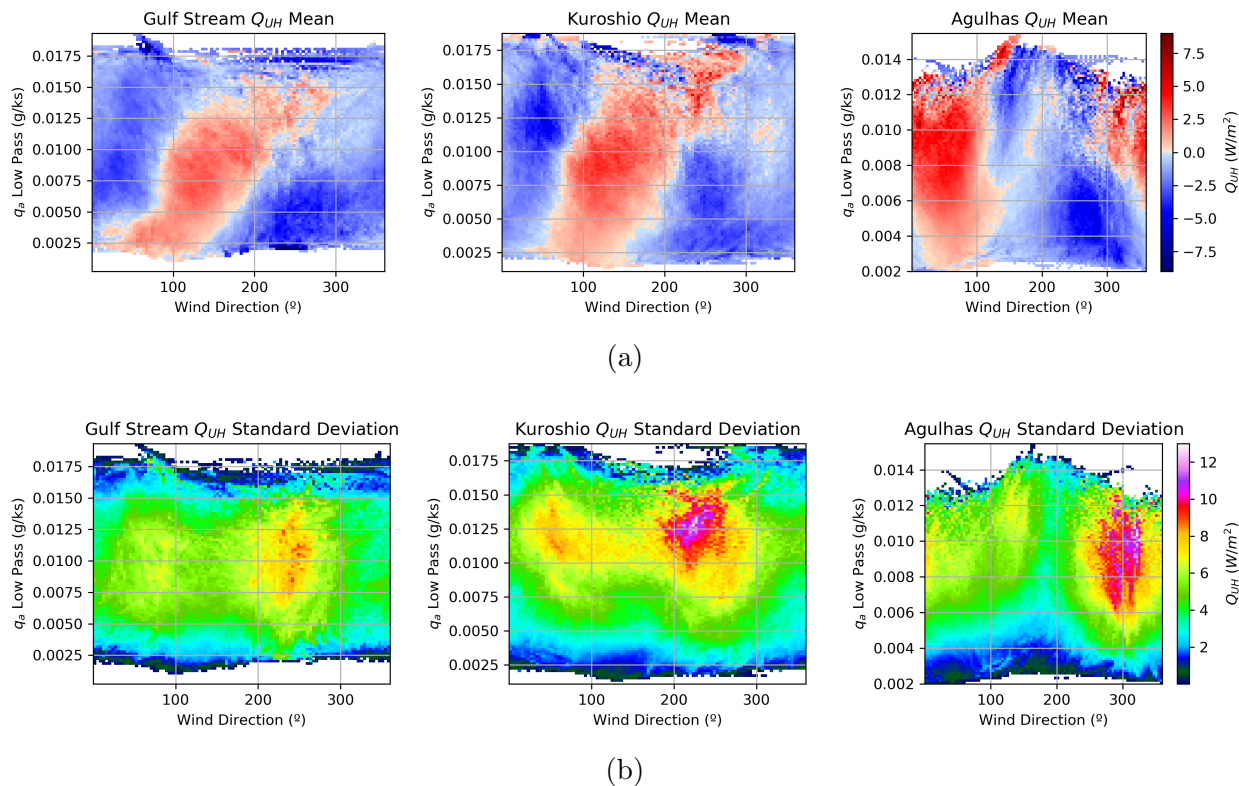


Figure 23: Trial 2. Dependence of the rectification of the covariability of wind speed and specific humidity (Q_{UH}) on background SST and background wind direction in the Gulf Stream, Kuroshio Extension, and Agulhas Return Current from 2003-2008. We took the mean (a) or standard deviation (b) of the rectification within each chosen SST and wind direction. The range of plot (a) was reduced to see the internal structure of the covariability. Zero degrees indicates wind blowing North.

	Gulf Stream (W/m^2)	Kuroshio (W/m^2)	Agulhas (W/m^2)
ε mean	3.03	2.33	4.11
ε max (95th%)	31.81 (10.64)	13.56 (4.72)	17.89 (7.71)
ε min (5th%)	-0.02 (0.15)	0.05 (0.81)	0.03 (1.46)

Table 5: Trial 2. Mean, maximum and 95th percentile, minimum and 5th percentile of ε across the entire data period in the Gulf Stream, Kuroshio Extension, and Agulhas Return Current.

suggests that there is a nonlinearity missing in our analysis.

One obvious nonlinearity that we did not consider is encapsulated in the constants in our LHF equation. We assigned the stability coefficient C_E as 1.3×10^{-3} , however, it is not actually constant (Wallace and Hobbs, 2006). There is also the drag coefficient, which

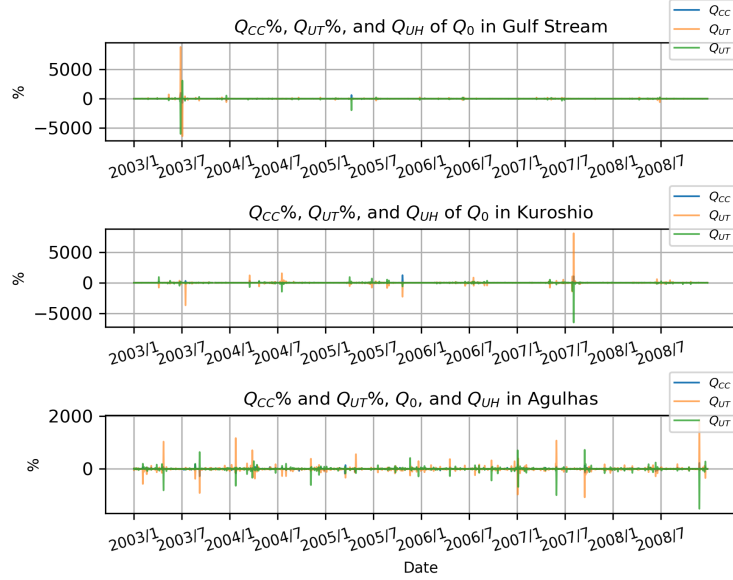


Figure 24: Trial 2. The daily average of the percentage the Clausius Clapeyron term (Q_{CC}), the covariability of wind speed and SST (Q_{UT}), and the covariability of wind speed and specific humidity (Q_{UH}) make up of the large scale LHF (Q_0).

affects the heat fluxes (Ma et al., 2017). Both of these coefficients are nonlinearly related to wind speed and, therefore, may also rectify mesoscale features to the large scale (Fairall et al., 2003). We will discuss this more in the Section 5.2.6.

We found that ε is directly related to the Clausius Clapeyron term but is completely independent of both covariability terms (see Figure 26). Only the Gulf Stream is plotted, but this relationship holds true in all three regions. This is only true for Trial 2; ε for Trial 1 is independent of the Clausius Clapeyron term. Because of this, ε has the same direct relationship that the Clausius Clapeyron term has on wind speed and SST standard deviation. This explains why the seasonal cycle of ε is in phase with the seasonal cycle of wind speed and the standard deviation of SST. ε is also independent of specific humidity and background SST just like the Clausius Clapeyron term is. This may be due to the Clausius Clapeyron effect appearing in higher order terms in the Taylor Expansion.

We also lose information by choosing to linearize around the specific humidity instead of relative humidity for our Taylor Expansion. We will explore this concept more in Section 5.2.5.

5.2.5 Linearize around Relative Humidity vs. Specific Humidity

For our Taylor Expansion, we linearized the LHF equation around a background state of SST, wind speed, and specific humidity. However, we can conduct the same calculations except utilize relative humidity instead of specific humidity. Relative humidity is the division of specific humidity over saturation humidity: $\phi = q_a/q_s$. We can alter our LHF Equation 9

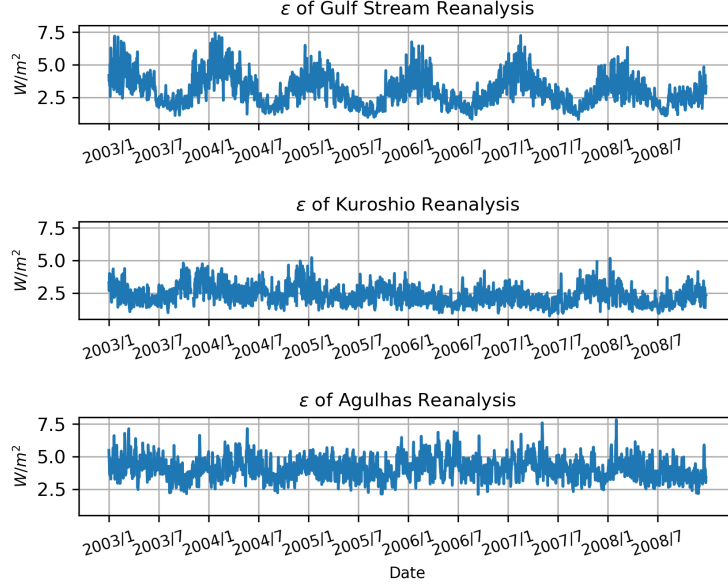


Figure 25: Trial 2. Daily average of ε in the Gulf Stream, Agulhas Return Current, and Kuroshio Extension with reanalysis data.

like so

$$Q_{LHF} = L_v \rho_a C_E |U_{10}| q_s (1 - \phi) \quad (9)$$

to change the independent variable from specific humidity to relative humidity. The new Taylor Expansion would be very similar to our Trial 2 version (Equation 7). However, the covariability of wind speed and specific humidity term becomes the covariability of wind speed and relative humidity

$$\underbrace{Q(\bar{T} + T', \bar{U} + U', \bar{\phi} + \phi')}_{Q_0 \text{ (Large-Scale)}} = \underbrace{Q(\bar{T}, \bar{U}, \bar{\phi})}_{Q_1 \text{ (Background State)}} + \underbrace{\frac{1}{2} \frac{\partial^2 Q}{\partial T^2} \Big|_{\bar{T}, \bar{U}, \bar{\phi}} \overline{T'^2}}_{Q_{CC} \text{ (Clausius Clapeyron)}} + \underbrace{\frac{\partial^2 Q}{\partial T \partial U} \Big|_{\bar{T}, \bar{U}, \bar{\phi}} \overline{T'U'}}_{Q_{UT} \text{ (Covariability)}} + \underbrace{\frac{\partial^2 Q}{\partial \phi \partial U} \Big|_{\bar{T}, \bar{U}, \bar{\phi}} \overline{\phi'U'}}_{Q_{UH} \text{ (Covariability)}} + \varepsilon. \quad (10)$$

This changes the second derivative in the covariability Q_{UH} term such that $\frac{\partial^2 Q}{\partial q_a \partial U}$ which was a constant, becomes $\frac{\partial^2 Q}{\partial \phi \partial U}$ which now depends on q_s and, therefore, SST. This added dependence on SST in our covariability Q_{UH} term could potentially reduce our large ε . This is an opportunity for further study.

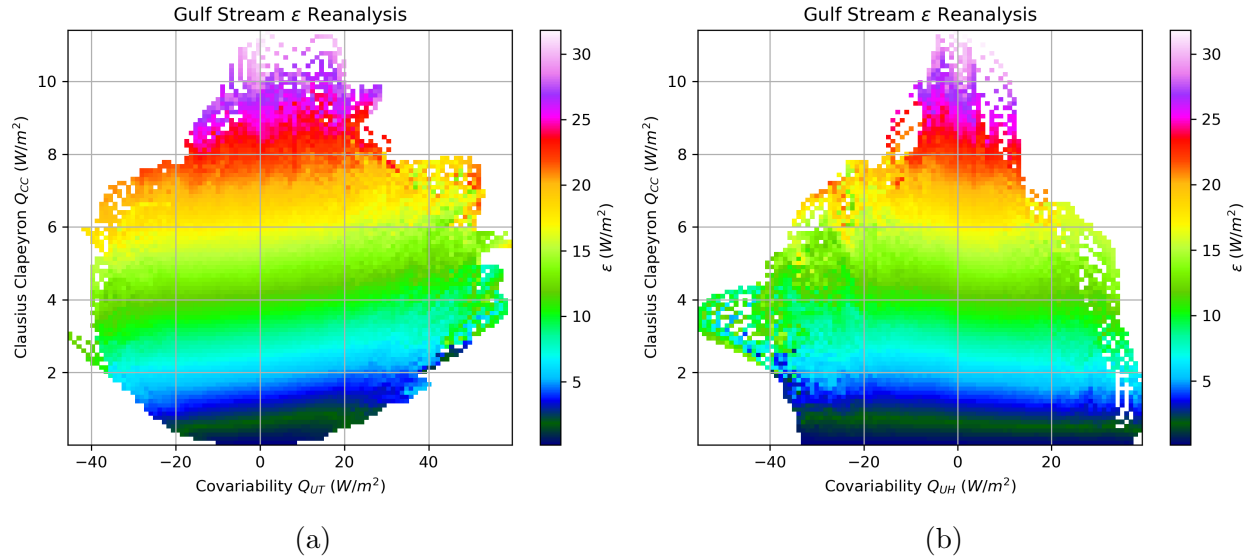


Figure 26: Trial 2. Dependence of the ϵ on the three rectification terms in the Gulf Stream from 2003-2008. Plot (a) is the dependence of ϵ on the Clausius Clapeyron term (Q_{CC}) and the covariability of wind speed and SST (Q_{UT}). Plot (b) is the dependence of ϵ on Q_{CC} and the covariability of wind speed and specific humidity Q_{UH} .

5.2.6 Drag and Stability Coefficients

The other nonlinearities that we did not consider in this study are the nonlinear constants in the LHF equation (Equation 1). They could also be contributing to our large ϵ . The bulk transfer coefficients for drag (C_D) and stability (or moisture) (C_E) are nonlinear (e.g., Ma et al., 2017; Liu et al., 2022; O’Neill et al., 2005; Smith, 1988); therefore, they could impact the rectification. They depend strongly on the sea-air virtual temperature difference at low wind speeds and they strongly depend on wind speed (Smith, 1988). A positive wind speed perturbation will alter the transfer coefficients a different amount compared to a negative wind speed perturbation, resulting in rectification. However, we set the stability coefficient C_E as a constant in our calculations, eliminating its effect on rectification (Smith, 1988; Wallace and Hobbs, 2006). We expect this missing nonlinearity to appear in our ϵ term.

The drag coefficient C_D is a well known, complicated nonlinearity. It impacts our LHF because it is used to calculate wind speed from wind stress data (Wallace and Hobbs, 2006). At very small wind speed (< 2 m/s) it decreases sharply. At very high wind speeds (< 35 m/s) there are conflicting studies that find the drag coefficient decreases or remains the same in increasing wind speeds (Ma et al., 2017). Generally, the drag coefficient increases with increasing wind speed (Smith, 1988). Studies confirm that the drag coefficient is nonlinear (e.g., Fairall et al., 2003; Ma et al., 2017; Liu et al., 2022; O’Neill et al., 2005; Smith, 1988). There is added complexity because the drag coefficient also impacts the stability coefficient C_E (Liu et al., 2022). The Quikscat scatterometer calculated their wind speed from wind stress by using a linear approximation of the drag coefficient that was recommended by

Smith (1988) (Ricciardulli et al., 2011). The ERA5 used a nonlinear, stability dependent drag coefficient that they calculated with the Charnock relation (for Medium-range Weather Forecasts , ECMWF). Thus, we would expect more information about the drag coefficient to be missing from the rectification in the Trial 1 analysis with Quikscat compared to the Trial 2 analysis with ERA5. This would lead us to expect a larger ε in Trial 1 compared to Trial 2, however, we found the opposite is true.

We briefly looked at the impact of the nonlinear coefficients by comparing the large scale LHF (Q_0) we calculated with the large scale LHF calculated by ERA5 (Hersbach et al., 2019b) in Figure 27. The LHF calculated by ERA5 used the same latent heat flux of evaporation (L_v), wind speed, and specific humidity as our calculation of LHF in Section 4.3 (for Medium-range Weather Forecasts , ECMWF). Their equation for calculating saturation humidity is different from ours, but similarly utilizes Teton’s formula and ERA5 SST (for Medium-range Weather Forecasts , ECMWF). Their density of air at sea level (ρ_a) is not constant, unlike ours. Their air density is calculated using virtual temperature and pressure with the basic state equation. The differences are small, (only about 2% variation in ρ_a) so it should have a minimal impact on the large scale LHF (for Medium-range Weather Forecasts , ECMWF). Their stability and drag coefficients adopt the Monin-Obukhov formulation and assume different roughness lengths for heat and momentum (for Medium-range Weather Forecasts , ECMWF).

Figure 27 compares the large scale LHF we calculated to the large scale LHF that ERA5 calculated. We smoothed the ERA5 LHF under the same 805 km top hat filter so that we compare the large scale for both. The differences between these two LHF should reveal the impacts of the drag and stability coefficient. The large scale LHF we calculated with a constant stability coefficient is smaller than the ERA5 large scale LHF by an average of $29.09 W/m^2$ in the Gulf Stream, $30.45 W/m^2$ in the Kuroshio Extension, and $23.71 W/m^2$ in the Agulhas Return Current. These values imply that the drag and stability coefficient increase the LHF by a substantial amount. If we were to use the true drag and stability coefficient instead of a constant in our Taylor Expansion, it is likely that of the magnitude of the rectification terms would also increase. Understanding the nonlinear drag and stability coefficients is an important course of study to fully understand the rectification of mesoscale ocean features to the large scale atmosphere.

6 Conclusion

The goal of this study was to quantify the the rectification of ocean mesoscale SST, wind speed, and specific humidity to the large-scale latent heat flux. We quantified three nonlinearities: Clausius Clapeyron, the covariability of wind speed and SST, and the covariability of wind speed and specific humidity. We quantified these three nonlinearities utilizing a Taylor Expansion to the second order of the latent heat flux around a background state of wind speed, SST, and specific humidity. We performed the study in two trials. Trial 1 utilized satellite data for wind speed and SST and estimated specific humidity to calculate the Clausius Clapeyron term and the covariability of wind speed and SST. Trial 2 utilized

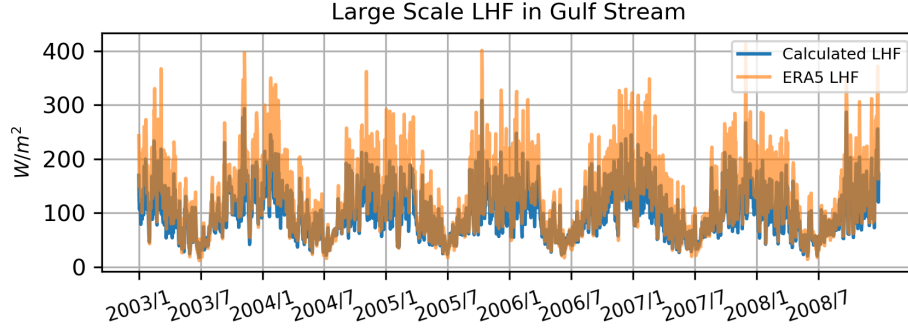


Figure 27: Trial 2. The daily average of large scale LHF and ε in the Gulf Stream. The blue line is the large scale LHF (Q_0) that we calculated in our Taylor expansion and the orange line is the LHF calculated by ERA5 which is then run through our low pass filter.

ERA5 reanalysis data for wind speed, SST, and specific humidity to calculate all three of the nonlinearities.

In Trial 1, the Clausius Clapeyron term and the covariability of wind speed and SST are small and make up only 1 - 2% of the large scale LHF on average. On average, the Clausius Clapeyron term is about 1 to 2 W/m^2 and the mean of the covariability of wind speed and SST ranges from -0.4 to 0.49 W/m^2 depending on the region. At the 5th and 95th percentile, the Clausius Clapeyron term ranges from 0.09 to 3.85 W/m^2 and the covariability term ranges from -4.06 to 4.39 W/m^2 . In Trial 2, the average of the Clausius Clapeyron term is about 0.78 to 1.36 W/m^2 , the covariability of wind speed and SST is -0.47 to 0.73 W/m^2 , and the covariability of wind speed and specific humidity is -0.68 to 0.61 W/m^2 depending on the region. From the 5th and 95th percentile the Clausius Clapeyron term ranges from 0.05 to 3.74 W/m^2 , the covariability of wind speed and SST ranges from -14.92 to 14.19 W/m^2 , and the the covariability of wind speed and specific humidity ranges from -9.30 to 7.91 W/m^2 . In both trials, the mean of the Clausius Clapeyron term is greater than the covariability terms; however, the range and daily variability of the covariability terms exceeds the Clausius Clapeyron term.

The Clausius Clapeyron term exhibits a strong dependence on background wind speed and SST standard deviation, however it is independent of background SST and wind direction. SST standard deviation and large-scale wind speed has a seasonal cycle that peaks in winter, thus, the Clausius Clapeyron term shares the same strong seasonal cycle. Events of large Clausius Clapeyron term are brief and only last for a day or so because large background wind speed is also brief.

The covariability of wind speed and SST depends on wind direction and the standard deviation of SST but is independent of background wind speed. The covariability term contains $\partial^2 Q / \partial T \partial U$, which directly relates to background SST and the covariance $\overline{T'U'}$ which indirectly relates to background SST. The covariability term exhibits no seasonal cycle because the background SST and $\overline{U'T'}$ are out of phase with one another. The magnitude of the covariability is greater during larger SST standard deviation, but the standard deviation

of SST does not inform the sign of the covariability. Wind direction has an impact on both the sign and the magnitude of the covariability, however, its dependence changes with the region of study. This is likely because the location of landmass and the equator and poles differ depending on the location of the study region.

The covariability of wind speed and specific humidity is independent of background SST, background specific humidity, and the standard deviation of SST, but exhibits dependence on background wind speed and wind direction. The covariability of wind speed and specific humidity is often negative in low wind speeds (< 10 m/s) and positive in high wind speeds (> 10 m/s). The magnitude of the covariability is greatest in moderate wind speeds (5 m/s to 15 m/s). Wind direction has an impact on both the sign and the magnitude of the covariability, however, it depends on the region of study. The sign of the covariability of wind speed and specific humidity at a particular wind speed is generally opposite to sign of the covariability of wind speed and SST at the same wind direction.

In both trials, the rectifications are greatest and exhibit the most variability in the Gulf Stream compared with the Kuroshio Extension and the Agulhas Return Current. The seasonal cycle is also strongest in the Gulf Stream. The large scale LHF is also the greatest in the Gulf Stream. This is possibly because the SST is the highest in the Gulf Stream compared to the other regions by about 3K on average. The rectification, seasonal cycle, and large scale LHF are all smallest in the Agulhas Return Current. This is likely due to the effect of less neighboring land coverage near the study region in the Agulhas Return Current compared to the other two regions. Overall, rectification mostly occurs over regions of strong SST variance. Instances of large rectification typically only last for 1-2 days; thus, high rectification events are likely caused by synoptic variability.

The results of Trial 1 are robust. ε , which encompasses the higher order terms and residuals, is an order of magnitude smaller than the rectification. This is an encouraging sign that our Taylor Expansion works and that the Clausius Clapeyron term and the covariability of wind speed and SST encompass all of the major nonlinearities in the large scale LHF. However, ε in Trial 2 is on the same order as the other rectification terms and exhibits a strong relationship to the Clausius Clapeyron term. We hypothesize that the Clausius Clapeyron effect occurs in the higher order Taylor Expansion terms. It is also likely that the drag and stability coefficients contain nonlinearities that we have not considered.

7 Discussion

The rectification of mesoscale ocean features to the large scale atmosphere has been estimated in a study by Sroka et al. (2022). In this study, they found that rectification from mesoscale eddies is small compared to the long-time large-spatial scale mean of the turbulent heat flux. They found it to be only a few W/m^2 and claim that it would be unlikely to surpass $10 W/m^2$. Their study looks at all of the turbulent heat fluxes combined while ours looks only at LHF, therefore, their results are likely larger than ours. Our results are consistent with theirs in Trial 1 because the sum of our two rectification terms (excluding ε) average to be about $1 W/m^2$ in Trial 1 and reach to 5 to $7 W/m^2$ in the 95th percentile.

In Trial 2, the sum of the three rectification terms (excluding ε) average to be about -0.5 to 1 W/m^2 , and they reach about 7 to 11 W/m^2 in the 95th percentile, depending on the region. They also found that the order of magnitude of the rectification is impacted by the strength of the large scale winds, the strength of the coupling between wind and SST anomalies, the low pass SST, and the strength of the mesoscale SST anomalies. Our project confirmed this; these variables impacted at least one of our nonlinearities and, therefore, the total rectification.

As noted above in the Sroka et al. (2022) study, LHF is not the only heat flux that rectifies mesoscale features to the large scale. We could also extend our research to include sensible heat flux (SHF). We could use the parameterization of the SHF by Fairall et al. (2003)

$$Q_{SHF} = \rho_a c_p C_H |U_{10}| (T_s - T_a). \quad (11)$$

The SHF equation contains the density of air at sea level (ρ_a), the heat exchange coefficient (C_H), the specific heat of air at constant pressure (c_p), wind speed (U_{10}), sea surface temperature (T_s), and air temperature T_a (Wallace and Hobbs, 2006). We could perform the Taylor Expansion around the SHF equation (Equation 11) to the second order around large scale SST, air temperature, and wind speed. We would expect the rectification from the SHF to be of similar magnitude to the rectification of the LHF. The SHF nonlinearities do not include the Clausius Clapeyron effect, but they would include the covariability of wind speed and SST, among others.

There could be numerous nonlinearities that rectify ocean mesoscale eddies to the large scale atmosphere. Our study successfully quantified three of them. A next step of this study would be to consider if these nonlinearities are sufficiently large to create the rectification seen by Ma et al. (2015), Piazza et al. (2016), and Foussard et al. (2019) studies. This could be quantified with numerical experiments. This is important because it ties our findings back into the exploration of ocean mesoscale sea surface temperature impact on the large-scale, mid-latitude atmosphere, and the storm tracks that govern weather and climate in the mid-latitudes.

References

- Bond, N. A. and Cronin, M. F. (2008). Regional weather patterns during anomalous air–sea fluxes at the Kuroshio Extension Observatory (KEO). *Journal of Climate*, 21(8):1680–1697.
- Cayan, D. R. (1992). Latent and sensible heat flux anomalies over the northern oceans: Driving the sea surface temperature. *Journal of Physical Oceanography*, 22(8):859–881.
- Chelton, D. B., Schlax, M. G., Freilich, M. H., and Milliff, R. F. (2004). Satellite measurements reveal persistent small-scale features in ocean winds. *science*, 303(5660):978–983.
- Chelton, D. B., Schlax, M. G., and Samelson, R. M. (2011). Global observations of nonlinear mesoscale eddies. *Progress in oceanography*, 91(2):167–216.

- Chelton, D. B. and Xie, S.-P. (2010). Coupled ocean-atmosphere interaction at oceanic mesoscales. *Oceanography*, 23(4):52–69.
- Fairall, C. W., Bradley, E. F., Hare, J., Grachev, A. A., and Edson, J. B. (2003). Bulk parameterization of air–sea fluxes: Updates and verification for the COARE algorithm. *Journal of Climate*, 16(4):571–591.
- for Medium-range Weather Forecasts), E. E. C. (2016). Part IV: Physical processes. *IFS Documentation–Cy41r2*, pages 1–213.
- Foussard, A., Lapeyre, G., and Plougonven, R. (2019). Storm track response to oceanic eddies in idealized atmospheric simulations. *Journal of Climate*, 32(2):445–463.
- Frenger, I., Gruber, N., Knutti, R., and Münnich, M. (2013). Imprint of Southern Ocean eddies on winds, clouds and rainfall. *Nature Geoscience*, 6(8):608–612.
- Hersbach, H., Bell, B., Berrisford, P., Biavati, G., Horányi, A., Muñoz Sabater, J., Nicolas, J., Peubey, C., Radu, R., Rozum, I., Schepers, D., Simmons, A., Soci, C., Dee, D., and Thépaut, J.-N. (2019a). ERA5 monthly averaged data on pressure levels from 1959 to present. *Copernicus Climate Change Service (C3S) Climate Data Store (CDS)*, Accessed on 21-07-2021.
- Hersbach, H., Bell, B., Berrisford, P., Biavati, G., Horányi, A., Muñoz Sabater, J., Nicolas, J., Peubey, C., Radu, R., Rozum, I., Schepers, D., Simmons, A., Soci, C., Dee, D., and Thépaut, J.-N. (2019b). ERA5 monthly averaged data on single levels from 1959 to present. *Copernicus Climate Change Service (C3S) Climate Data Store (CDS)*, Accessed on 21-07-2021.
- Laurindo, L. C., Siqueira, L., Mariano, A. J., and Kirtman, B. P. (2019). Cross-spectral analysis of the SST/10-m wind speed coupling resolved by satellite products and climate model simulations. *Climate Dynamics*, 52(9):5071–5098.
- Leyba, I. M., Saraceno, M., and Solman, S. A. (2017). Air-sea heat fluxes associated to mesoscale eddies in the Southwestern Atlantic Ocean and their dependence on different regional conditions. *Climate Dynamics*, 49(7):2491–2501.
- Liu, H., Li, W., Chen, S., Fang, R., and Li, Z. (2018). Atmospheric response to mesoscale ocean eddies over the South China Sea. *Advances in Atmospheric Sciences*, 35(9):1189–1204.
- Liu, L., Wang, G., Zhang, Z., and Wang, H. (2022). Effects of Drag Coefficients on Surface Heat Flux during Typhoon Kalmaegi (2014). *Advances in Atmospheric Sciences*, pages 1–18.
- Liu, Y., Yu, L., and Chen, G. (2020). Characterization of sea surface temperature and air-sea heat flux anomalies associated with mesoscale eddies in the South China Sea. *Journal of Geophysical Research: Oceans*, 125(4):e2019JC015470.

- Ma, X., Chang, P., Saravanan, R., Montuoro, R., Hsieh, J.-S., Wu, D., Lin, X., Wu, L., and Jing, Z. (2015). Distant influence of Kuroshio eddies on North Pacific weather patterns? *Scientific Reports*, 5(1):1–7.
- Ma, Y., Davidson, N. E., Xiao, Y., and Bao, J.-W. (2017). Revised parameterization of air–sea exchanges in high winds for operational numerical prediction: Impact on tropical cyclone track, intensity, and rapid intensification. *Weather and Forecasting*, 32(3):821–848.
- O’Neill, L. W., Chelton, D. B., and Esbensen, S. K. (2010). The effects of SST-induced surface wind speed and direction gradients on midlatitude surface vorticity and divergence. *Journal of Climate*, 23(2):255–281.
- O’Neill, L. W., Chelton, D. B., Esbensen, S. K., and Wentz, F. J. (2005). High-resolution satellite measurements of the atmospheric boundary layer response to sst variations along the Agulhas Return Current. *Journal of Climate*, 18(14):2706–2723.
- Piazza, M., Terray, L., Boé, J., Maisonnave, E., and Sanchez-Gomez, E. (2016). Influence of small-scale North Atlantic sea surface temperature patterns on the marine boundary layer and free troposphere: A study using the atmospheric ARPEGE model. *Climate dynamics*, 46(5):1699–1717.
- Putrasahan, D. A., Miller, A. J., and Seo, H. (2013). Isolating mesoscale coupled ocean–atmosphere interactions in the Kuroshio Extension region. *Dynamics of Atmospheres and Oceans*, 63:60–78.
- Ricciardulli, L., Wentz, F. J., and Smith, D. K. (2011). Remote Sensing Systems QuikSCAT 2011 daily, ocean vector winds on 0.25 deg grid, version 4. Available online at www.remss.com/missions/qscat.
- Santorelli, A., Pinker, R., Bentamy, A., Katsaros, K., Drennan, W., Mestas-Nuñez, A., and Carton, J. (2011). Differences between two estimates of air-sea turbulent heat fluxes over the Atlantic Ocean. *Journal of Geophysical Research: Oceans*, 116(C9).
- Shaman, J., Samelson, R., and Skillingstad, E. (2010). Air–sea fluxes over the Gulf Stream region: Atmospheric controls and trends. *Journal of Climate*, 23(10):2651–2670.
- Small, R. d., deSzoeko, S. P., Xie, S., O’neill, L., Seo, H., Song, Q., Cornillon, P., Spall, M., and Minobe, S. (2008). Air–sea interaction over ocean fronts and eddies. *Dynamics of Atmospheres and Oceans*, 45(3-4):274–319.
- Smith, S. D. (1988). Coefficients for sea surface wind stress, heat flux, and wind profiles as a function of wind speed and temperature. *Journal of Geophysical Research: Oceans*, 93(C12):15467–15472.
- Sroka, S., Czaja, A., and Chakravorty, S. (2022). Assessing the importance of mesoscale sea surface temperature variations for surface turbulent cooling of the Kuroshio Extension in wintertime. Unpublished Manuscript.

- Villas Bôas, A., Sato, O., Chaigneau, A., and Castelão, G. (2015). The signature of mesoscale eddies on the air-sea turbulent heat fluxes in the South Atlantic ocean. *Geophysical Research Letters*, 42(6):1856–1862.
- Wallace, J. M. and Hobbs, P. V. (2006). *Atmospheric Science An Introductory Survey*. Elsevier Inc, 2 edition.
- Wentz, F., Meissner, T., Gentemann, C., and M. (2014). Remote Sensing Systems AQUA AMSR-E 3-day environmental suite on 0.25 deg grid, version V.7. Available online at www.remss.com/missions/amsr.